in mitochondrial SQR enzymes are well conserved in this enzyme and it produces high levels of ROS. Absence of complex III and IV activities in its respiratory chain is an additional advantage of this model. Analysis of its crystal structure and expression of its subunits in a cell-free system for mutational analysis are in progress. These studies will provide further insight into the possibility of high levels of ROS production from both the FAD site and the Q site in the complex II of *A. suum* adult worm and help to understand the role of mutations in human complex II for carcinogenesis.

Acknowledgements

This work was supported by a grant-in-aid for scientific research on Priority Areas (18073004), Creative Scientific Research (18GS0314), and Targeted Proteins Research Program to KK and by a Japanese Government scholarship to MPP from the Japanese Ministry of Education, Science, Culture, Sports and Technology.

References

Ackrell, B.A., 2002. Cytopathies involving mitochondrial complex II. Mol. Aspects. Med. 23, 369–384.

Amino, H., Osanai, A., Miyadera, H., Shinjyo, N., Tomitsuka, E., Taka, H., Mineki, R., Murayama, K., Takamiya, S., Aoki, T., Miyoshi, H., Sakamoto, K., Kojima, S., Kita, K., 2003. Isolation and characterization of the stage-specific cytochrome b small subunit (CybS) of *Ascaris suum* complex II from the aerobic respiratory chain of larval mitochondria. Mol. Biochem. Parasitol. 128, 175–186.

Amino, H., Wang, H., Hirawake, H., Saruta, F., Mizuchi, D., Mineki, R., Shindo, N., Murayama, K., Takamiya, S., Aoki, T., Kojima, S., Kita, K., 2000. Stage-specific isoforms of *Ascaris suum* complex. II: The fumarate reductase of the parasitic adult and the succinate dehydrogenase of free-living larvae share a common iron–sulfur subunit. Mol. Biochem. Parasitol. 106, 63–76.

Astuti, D., Latif, F., Dallol, A., Dahia, P.L., Douglas, F., George, E., Skoldberg, F., Husebye, E.S., Eng, C., Maher, E.R., 2001. Gene mutations in the succinate dehydrogenase subunit SDHB cause susceptibility to familial pheochromocytoma and to familial paraganglioma. Am. J. Hum. Genet. 69, 49–54.

Azzi, A., Montecucco, C., Richter, C., 1975. The use of acetylated ferricytochrome c for the detection of superoxide radicals produced in biological membranes. Biochem. Biophys. Res. Commun. 65, 597–603.

Bayley, J.P., van Minderhout, I., Weiss, M.M., Jansen, J.C., Oomen, P.H., Menko, F.H., Pasini, B., Ferrando, B., Wong, N., Alpert, L.C., Williams, R., Blair, E., Devilee, P., Taschner, P.E., 2006. Mutation analysis of SDHB and SDHC: novel germline mutations in sporadic head and neck paraganglioma and familial paraganglioma and/or pheochromocytoma. BMC Med. Genet. doi:10-1186/1471-2350-7-1.

Baysal, B.E., Ferrell, R.E., Willett-Brozick, J.E., Lawrence, E.C., Myssiorek, D., Bosch, A., van der Mey, A., Taschner, P.E., Rubinstein, W.S., Myers, E.N., Richard 3rd, C.W., Cornelisse, C.J., Devilee, P., Devlin, B., 2000. Mutations in SDHD, a mitochondrial complex II gene, in hereditary paraganglioma. Science 287, 848–851.

Baysal, B.E., Willett-Brozick, J.E., Lawrence, E.C., Drovdlic, C.M., Savul, S.A., McLeod, D.R., Yee, H.A., Brackmann, D.E., Slattery 3rd, W.H., Myers, E.N., Ferrell, R.E., Rubinstein, W.S., 2002. Prevalence of SDHB, SDHC, and SDHD germline mutations in clinic patients with head and neck paragangliomas. J. Med. Genet. 39, 178–183.

Bourgeron, T., Rustin, P., Chretien, D., Birch-Machin, M., Bourgeois, M., Viegas-Pequignot, E., Munnich, A., Rotig, A., 1995. Mutation of a nuclear succinate dehydrogenase gene results in mitochondrial respiratory chain deficiency. Nat. Genet. 11, 144–149.

Briere, J.J., Favier, J., Benit, P., El Ghouzzi, V., Lorenzato, A., Rabier, D., Di Renzo, M.F., Gimenez-Roqueplo, A.P., Rustin, P., 2005. Mitochondrial succinate is instrumental for HIF1alpha nuclear translocation in SDHA-mutant fibroblasts under normoxic conditions. Hum. Mol. Genet. 14, 3263–3269.

Cecchini, G., Schroder, I., Gunsalus, R.P., Maklashina, E., 2002. Succinate dehydrogenase and fumarate reductase from *Escherichia coli*. Biochim. Biophys. Acta. 1553, 140–157.

Cervera, A.M., Apostolova, N., Crespo, F.L., Mata, M., McCreath, K.J., 2008. Cells silenced for SDHB expression display characteristic features of the tumor phenotype. Cancer Res. 68, 4058–4067.

Chen, Q., Vazquez, E.J., Moghaddas, S., Hoppel, C.L., Lesnefsky, E.J., 2003. Production of reactive oxygen species by mitochondria: central role of complex III. J. Biol. Chem. 278, 36027–36031.

Eng, C., Kiuru, M., Fernandez, M.J., Aaltonen, L.A., 2003. A role for mitochondrial enzymes in inherited neoplasia and beyond. Nat. Rev. Cancer 3, 193–202.

Eto, Y., Kang, D., Hasegawa, E., Takeshige, K., Minakami, S., 1992. Succinate-dependent lipid peroxidation and its prevention by reduced ubiquinone in beef heart submitochondrial particles. Arch. Biochem. Biophys. 295, 101–106.

Guo, J., Lemire, B.D., 2003. The ubiquinone-binding site of the *Saccharomyces cerevisiae* succinate–ubiquinone oxidoreductase is a source of superoxide. J. Biol. Chem. 278, 47629–47635.

Guzy, R.D., Sharma, B., Bell, E., Chandel, N.S., Schumacker, P.T., 2008. Loss of the SdhB, but Not the SdhA, subunit of complex II triggers reactive oxygen species-dependent hypoxia-inducible factor activation and tumorigenesis. Mol. Cell Biol. 28, 718–731.

Hirst, J., King, M.S., Pryde, K.R., 2008. The production of reactive oxygen species by complex I. Biochem. Soc. Trans. 36, 976–980.

Horsefield, R., Yankovskaya, V., Sexton, G., Whittingham, W., Shiomi, K., Omura, S., Byrne, B., Cecchini, G., Iwata, S., 2006. Structural and computational analysis of the quinone-binding site of complex II (succinate–ubiquinone oxidoreductase): a mechanism of electron transfer and proton conduction during ubiquinone reduction. J. Biol. Chem. 281, 7309–7316.

Huang, J., Lemire, B.D., 2009. Mutations in the *C. elegans* succinate dehydrogenase iron-sulfur subunit promote superoxide generation and premature aging. J. Mol. Biol. 387, 559–569.

Huang, L.S., Shen, J.T., Wang, A.C., Berry, E.A., 2006. Crystallographic studies of the binding of ligands to the dicarboxylate site of Complex II, and the identity of the ligand in the "oxaloacetate-inhibited" state. Biochim. Biophys. Acta 1757, 1073–1083.

Imlay, J.A., Fridovich, I., 1991. Assay of metabolic superoxide production in *Escherichia coli*. J. Biol. Chem. 266, 6957–6965.

Indo, H.P., Davidson, M., Yen, H.C., Suenaga, S., Tomita, K., Nishii, T., Higuchi, M., Koga, Y., Ozawa, T., Majima, H.J., 2007. Evidence of ROS generation by mitochondria in cells with impaired electron transport chain and mitochondrial DNA damage. Mitochondrion 7, 106–118.

Ishii, T., Sakurai, T., Usami, H., Uchida, K., 2005. Oxidative modification of proteasome: identification of an oxidation-sensitive subunit in 26S proteasome. Biochemistry 44, 13893–13901.

Iwata, F., Shinjyo, N., Amino, H., Sakamoto, K., Islam, M.K., Tsuji, N., Kita, K., 2008. Change of subunit composition of mitochondrial complex II (succinate–ubiquinone reductase/quinol-fumarate reductase) in *Ascaris suum* during the migration in the experimental host. Parasitol. Int. 57, 54–61.

Jezek, P., Hlavata, L., 2005. Mitochondria in homeostasis of reactive oxygen species in cell, tissues, and organism. Int. J. Biochem. Cell Biol. 37, 2478–2503.

Kita, K., Hirawake, H., Miyadera, H., Amino, H., Takeo, S., 2002. Role of complex II in anaerobic respiration of the parasite mitochondria from *Ascaris suum* and *Plasmodium falciparum*. Biochim. Biophys. Acta 1553, 123–139.

Kita, K., Takamiya, S., 2002. Electron-transfer complexes in Ascaris mitochondria. Adv. Parasitol. 51, 95–131.

Kita, K., Shiomi, K., Õmura, S., 2007. Parasitology in Japan: advances in drug discovery and biochemical studies. Trends. Parasitol. 23, 223–229.

Kuramochi, T., Hirawake, H., Kojima, S., Takamiya, S., Furushima, R., Aoki, T., Komuniecki, R., Kita, K., 1994. Sequence comparison between the flavoprotein subunit of the fumarate reductase (complex II) of the anaerobic parasitic nematode, *Ascaris suum* and the succinate dehydrogenase of the aerobic, free-living nematode, *Caenorhabditis elegans*. Mol. Biochem. Parasitol. 68, 177–187.

Lancaster, C.R.D., 2004. Structure and function of succinate: quinone oxidoreductases and the role of quinol: fumarate reductases in fumarate respiration. In: Zannoni, D. (Ed.), Respiration in Archaea and Bacteria: Diversity of Prokaryotic Electron Transport Carriers. Kluwer Academic Publishers, The Netherlands, pp. 57–85.

Liu, Y., Fiskum, G., Schubert, D., 2002. Generation of reactive oxygen species by the mitochondrial electron transport chain. J. Neurochem. 80, 780–787.

Lowry, O.H., Rosebrough, N.J., Farr, A.L., Randall, R.J., 1951. Protein measurement with the Folin phenol reagent. J. Biol. Chem. 193, 265–275.

Matsumoto, J., Sakamoto, K., Shinjyo, N., Kido, Y., Yamamoto, N., Yagi, K., Miyoshi, H., Nonaka, N., Katakura, K., Kita, K., Oku, Y., 2008. Anaerobic NADH-fumarate reductase system is predominant in the respiratory chain of *Echinococcus multilocularis*, providing a novel target for the chemotherapy of alveolar echinococcosis. Antimicrob. Agents Chemother. 52, 164–170.

Matsuno-Yagi, A., Hatefi, Y., 1985. Studies on the mechanism of oxidative phosphorylation. Catalytic site cooperativity in ATP synthesis. J. Biol. Chem. 260, 11424–11427.

Messner, K.R., Imlay, J.A., 2002. Mechanism of superoxide and hydrogen peroxide formation by fumarate reductase, succinate dehydrogenase, and aspartate oxidase. J. Biol. Chem. 277, 42563–42571.

Miyadera, H., Shiomi, K., Ui, H., Yamaguchi, Y., Masuma, R., Tomoda, H., Miyoshi, H., Osanai, A., Kita, K., Omura, S., 2003. Atpenins, potent and specific inhibitors of mitochondrial complex II (succinate–ubiquinone oxidoreductase). Proc. Natl. Acad. Sci. USA 100, 473–477.

Mohanty, J.G., Jaffe, J.S., Schulman, E.S., Raible, D.G., 1997. A highly sensitive fluorescent micro-assay of H2O2 release from activated human leukocytes using a dihydroxyphenoxazine derivative. J. Immunol. Methods 202, 133–141.

Muller, F.L., Liu, Y., Abdul-Ghani, M.A., Lustgarten, M.S., Bhattacharya, A., Jang, Y.C., Van Remmen, H., 2008. High rates of superoxide production in skeletal-muscle mitochondria respiring on both complex I- and complex II-linked substrates. Biochem. J. 409, 491–499.

Murphy, M.P., 2009. How mitochondria produce reactive oxygen species. Biochem. J. 417, 1–13.

Ni, Y., Zbuk, K.M., Sadler, T., Patocs, A., Lobo, G., Edelman, E., Platzer, P., Orloff, M.S., Waite, K.A., Eng, C., 2008. Germline mutations and variants in the succinate dehydrogenase genes in Cowden and Cowden-like syndromes. Am. J. Hum. Genet. 83, 261–268.

Paddenberg, R., Ishaq, B., Goldenberg, A., Faulhammer, P., Rose, F., Weissmann, N., Braun-Dullaeus, R.C., Kummer, W., 2003. Essential role of complex II of the respiratory chain in hypoxia-induced ROS generation in the pulmonary vasculature. Am. J. Physiol. Lung. Cell. Mol. Physiol. 284, L710–719.

Saruta, F., Hirawake, H., Takamiya, S., Ma, Y.C., Aoki, T., Sekimizu, K., Kojima, S., Kita, K., 1996. Cloning of a cDNA encoding the small subunit of cytochrome b558 (cybS) of mitochondrial fumarate reductase (complex II) from adult *Ascaris suum*. Biochim. Biophys. Acta. 1276, 1–5.

Saruta, F., Kuramochi, T., Nakamura, K., Takamiya, S., Yu, Y., Aoki, T., Sekimizu, K., Kojima, S., Kita, K., 1995. Stage-specific isoforms of complex II (succinate–ubiquinone oxidoreductase) in mitochondria from the parasitic nematode, *Ascaris suum*. J. Biol. Chem. 270, 928–932.

Senoo-Matsuda, N., Yasuda, K., Tsuda, M., Ohkubo, T., Yoshimura, S., Nakazawa, H., Hartman, P.S., Ishii, N., 2001. A defect in the cytochrome b large subunit in complex II causes both superoxide anion overproduction and abnormal energy metabolism in *Caenorhabditis elegans*. J. Biol. Chem. 276, 41553–41558.

Selak, M.A., Armour, S.M., MacKenzie, E.D., Boulahbel, H., Watson, D.G., Mansfield, K.D., Pan, Y., Simon, M.C., Thompson, C.B., Gottlieb, E., 2005. Succinate links TCA cycle dysfunction to oncogenesis by inhibiting HIF-alpha prolyl hydroxylase. Cancer Cell 7, 77–85.

Shinjyo, N., Kita, K., 2007. Relationship between reactive oxygen species and heme metabolism during the differentiation of Neuro2a cells. Biochem. Biophys. Res. Commun. 358, 130–135.

St-Pierre, J., Buckingham, J.A., Roebuck, S.J., Brand, M.D., 2002. Topology of superoxide production from different sites in the mitochondrial electron transport chain. J. Biol. Chem. 277, 44784–44790.

Sun, F., Huo, X., Zhai, Y., Wang, A., Xu, J., Su, D., Bartlam, M., Rao, Z., 2005. Crystal structure of mitochondrial respiratory membrane protein complex II. Cell 121, 1043–1057.

Szeto, S.S., Reinke, S.N., Sykes, B.D., Lemire, B.D., 2007. Ubiquinone-binding site mutations in the *Saccharomyces cerevisiae* succinate dehydrogenase generate superoxide and lead to the accumulation of succinate. J. Biol. Chem. 282, 27518–27526.

Takamiya, S., Furushima, R., Oya, H., 1986. Electron transfer complexes of Ascaris suum muscle mitochondria. II. Succinate–coenzyme Q reductase (complex II) associated with substrate-reducible cytochrome *b*558. Biochim. Biophys. Acta 848, 99–107.

Van Hellmond, J.J., van der Klei, A., van Weelden, S.W.H., Tielens, A.G.M., 2003. Biochemical and evolutionary aspects of anaerobically functioning bacteria. Phil. Trans. R. Soc. B. 358, 205–215.

Yamashita, T., Ino, T., Miyoshi, H., Sakamoto, K., Osanai, A., Nakamaru-Ogiso, E., Kita, K., 2004. Rhodoquinone reaction site of mitochondrial complex I, in parasitic helminth, *Ascaris suum*. Biochim. Biophys. Acta 1608, 97–103.

Yankovskaya, V., Horsefield, R., Tornroth, S., Luna-Chavez, C., Miyoshi, H., Leger, C., Byrne, B., Cecchini, G., Iwata, S., 2003. Architecture of succinate dehydrogenase and reactive oxygen species generation. Science 299, 700–704.

Zhang, L., Yu, L., Yu, C.A., 1998. Generation of superoxide anion by succinate–cytochrome c reductase from bovine heart mitochondria. J. Biol. Chem. 273, 33972–33976.

Zhao, Z., Rothery, R.A., Weiner, J.H., 2006. Effects of site-directed mutations in *Escherichia coli* succinate dehydrogenase on the enzyme activity and production of superoxide radicals. Biochem. Cell Biol. 84, 1013–1021.

AUTHOR QUERY FORM

ELSEVIER	**Journal: PARINT** **Article Number: 757**	**Please e-mail or fax your responses and any corrections to:** **E-mail: corrections.esch@elsevier.spitech.com** **Fax: +1 61 9699 6721**

Dear Author,

Any queries or remarks that have arisen during the processing of your manuscript are listed below and highlighted by flags in the proof. Please check your proof carefully and mark all corrections at the appropriate place in the proof (e.g., by using on-screen annotation in the PDF file) or compile them in a separate list.

For correction or revision of any artwork, please consult http://www.elsevier.com/artworkinstructions.

Articles in Special Issues: Please ensure that the words 'this issue' are added (in the list and text) to any references to other articles in this Special Issue.

Uncited references: References that occur in the reference list but not in the text – please position each reference in the text or delete it from the list.	
Missing references: References listed below were noted in the text but are missing from the reference list – please make the list complete or remove the references from the text.	
Location in article	**Query / remark** **Please insert your reply or correction at the corresponding line in the proof**
Q1	Uncited reference: This section comprises references that occur in the reference list but not in the body of the text. Please position each reference in the text or, alternatively, delete it. Any reference not dealt with will be retained in this section. Thank you.
Q2	Please update the status of this reference by providing issue number and pagination details.
Q3	Please update the status of this reference by providing volume number, issue and pagination details or DOI.

Electronic file usage
Sometimes we are unable to process the electronic file of your article and/or artwork. If this is the case, we have proceeded by:

☐ Scanning (parts of) your article ☐ Rekeying (parts of) your article ☐ Scanning the artwork

Thank you for your assistance.

Table S1 *P. falciparum, P. marinus, C. muris, C. parvum* and *T. vaginalis* mitochondrial proteins.

Table S2 Predicted subunits of *T. brucei* NDH1.

Fig. S1 Proposed metabolic pathways in *T. vaginalis* hydrogenosome.

ARTICLE IN PRESS

PARINT-00757; No of Pages 8

Parasitology International xxx (2010) xxx–xxx

Contents lists available at ScienceDirect

Parasitology International

journal homepage: www.elsevier.com/locate/parint

Mini-review

Diversity in mitochondrial metabolic pathways in parasitic protists *Plasmodium* and *Cryptosporidium*

Tatsushi Mogi *, Kiyoshi Kita *

Department of Biomedical Chemistry, Graduate School of Medicine, the University of Tokyo, Hongo, Bunkyo-ku, Tokyo 113-0033, Japan

ARTICLE INFO

Article history:
Received 12 February 2009
Received in revised form 24 September 2009
Accepted 25 September 2009
Available online xxxx

Keywords:
Apicomplexa
ATP synthesis
Metabolism
Mitochondria
Mitosome
Parasitic protists

ABSTRACT

Apicomplexans are obligate intracellular parasites and occupy diverse niches. They have remodeled mitochondrial carbon and energy metabolism through reductive evolution. *Plasmodium* lacks mitochondrial pyruvate dehydrogenase and H^+-translocating NADH dehydrogenase (Complex I, NDH1). The mitochondrion contains a minimal mtDNA (~6 kb) and carries out oxidative phosphorylation in the insect vector stages, by using 2-oxoglutarate as an alternative means of entry into the TCA cycle and a single-subunit flavoprotein as an alternative NADH dehydrogenase (NDH2). In the blood stages of mammalian hosts, mitochondrial enzymes are down-regulated and parasite energy metabolism relies mainly on glycolysis. Mitosomes of *Cryptosporidium parvum* and *Cryptosporidium hominis* (human intestine parasites) lack mtDNA, pyruvate dehydrogenase, TCA cycle enzymes except malate-quinone oxidoreductase (MQO), and ATP synthase subunits except α and β. In contrast, mitosomes of *Cryptosporidium muris* (a rodent gastric parasite) retain all TCA cycle enzymes and functional ATP synthase and carry out oxidative phosphorylation with pyruvate-$NADP^+$ oxidoreductase (PNO) and a simple and unique respiratory chain consisting of NDH2 and alternative oxidase (AOX). *Cryptosporidium* and *Perkinsus* are early branching groups of chromoalveolates (apicomplexa and dinoflagellates, respectively), and both *Cryptosporidium* mitosome and *Perkinsus* mitochondrion use PNO, MQO, and AOX. All apicomplexan parasites and dinoflagellates share MQO, which has been acquired from ε-proteobacteria *via* lateral gene transfer. By genome data mining on *Plasmodium*, *Cryptosporidium* and *Perkinsus*, here we summarized their mitochondrial metabolic pathways, which are varied largely from those of mammalian hosts. We hope that our findings will help in understanding the apicomplexan metabolism and development of new chemotherapeutics with novel targets.

Contents

Abbreviations: 2OG, 2-oxoglutarate; 2OGDH, 2-oxoglutarate dehydrogenase; ACS, acetyl-CoA synthase; ANT, adenine nucleotide transporter; AOX, alternative oxidase; AOXL, AOX-like proteins; BCKDH, branched-chain ketoacid dehydrogenase; COX, cytochrome *c* oxidase; DHOD, dihydroorotate dehydrogenase; FDP, flavodiiron protein; Fdx, ferredoxin; ICDH, isocitrate dehydrogenase; MDH, NAD-dependent malate dehydrogenase; ME, malic enzyme; MQO, malate-quinone oxidoreductase; NDH1, H^+-translocating NADH dehydrogenase complex; NDH2, a single-subunit NADH dehydrogenase; OSCP, oligomycin-sensitivity conferring protein; PDH, pyruvate dehydrogenase; PFO, pyruvate-ferredoxin oxidoreductase; PNO, pyruvate-$NADP^+$ oxidoreductase; PTOX, plastid terminal oxidase; Q, ubiquinone; QCR, ubiquinol-cytochrome *c* reductase; SCS, succinyl-CoA synthase; SDH, succinate dehydrogenase; SOD, superoxide dismutase; TCA, tricarboxylic acid; TH, NAD(P) transhydrogenase; Trx, thioredoxin; TrxP, thioredoxin peroxidase.

* Corresponding authors. Fax: +81 3 5841 3444.
E-mail addresses: tmogi@m.u-tokyo.ac.jp (T. Mogi), kitak@m.u-tokyo.ac.jp (K. Kita).

1383-5769/$ – see front matter © 2010 Published by Elsevier Ireland Ltd.
doi:10.1016/j.parint.2010.04.005

Please cite this article as: Mogi T, Kita K, Diversity in mitochondrial metabolic pathways in parasitic protists *Plasmodium* and *Cryptosporidium*, Parasitol Int (2010), doi:10.1016/j.parint.2010.04.005

1. Introduction

Apicomplexan parasites include the causative agents for malaria (*Plasmodium*), babesiosis (*Babesia*), East Coast cattle fever and tropical theileriosis (*Theileria*), toxoplasmosis (*Toxoplasma*), cryptosporidiosis (*Cryptosporidium*), and coccidiosis (*Eimeria*). Apicomplexan parasites are evolutionarily related to dinoflagellates. They diverged at least 400 million years ago, and although many dinoflagellates have retained photosynthesis, apicomplexans have lost this ability. The basal groups are assumed to be *Cryptosporidium* and gregarines with respect to hemosporidians and coccidians [1]. All apicomplexan species except *Cryptosporidium* species and some gregarines harbor a semiautonomous plastid-like organelle termed the apicoplast, which was derived *via* secondary endosymbiosis of a red alga and is indispensable to the parasites [2].

Apicomplexans are obligate intracellular parasites and occupy diverse niches. During the life cycle they undergo morphological and metabolic changes upon destinations in hosts. Further two-host parasites need to adapt to different habitats. During reductive evolution, parasites have remodeled mitochondrial carbon and energy metabolism. *Cryptosporidium* species have lost mtDNA and most mitochondrial functions [3] while other apicomplexan species retained a minimal mtDNA (~6 kb in *Plasmodium*), TCA cycle enzymes, and respiratory chain complexes except H^+-translocating NADH dehydrogenase complex (NDH1[1], Complex I). NDH1 is substituted by a single-subunit NADH dehydrogenase (NDH2), which binds peripherally to the inner membrane. *Cryptosporidium* lacks both ubiquinol-cytochrome *c* reductase (QCR, Complex III) and cytochrome *c* oxidase (COX, Complex IV) and uses alternative oxidase (AOX), which binds peripherally to the inner membrane and directly oxidizes ubiquinol with molecular oxygen.

Plasmodium and piroplasm parasites undergo a complex life cycle that involves both arthropod vectors and vertebrate hosts. *Plasmodium* and the piroplasms *Theileria* and *Babesia* infect blood cells and are transmitted by blood-sucking vectors (insects and ticks, respectively) to vertebrates. *Plasmodium* shows multiple tissue trophisms and transformation through multiple developmental stages, such as hepatocyte invasion and intrahepatocytic schizogony [4]. In the insect stages, parasites can use amino acids as a carbon source [5]. In the asexual mammalian stages, mitochondrial energy transduction systems for oxidative phosphorylation are down-regulated and parasites produce ATP mainly *via* glycolysis by using blood glucose [6,7]. Accordingly, parasites need to remodel metabolic systems upon parasitic adaptation to host environments. All analyzed apicomplexan species except *Cryptosporidium parvum* and *Cryptosporidium hominis* contain a complete set of tricarboxylic acid (TCA) cycle genes (Fig. 1, Table S1) [10–17]. Notably, the *Babesia* [10] and *Plasmodium* [11,12] genomes encode a single pyruvate dehydrogenase (PDH) complex, which is exclusively localized in the apicoplast [13,14] while *Theileria* genomes do not encode all the subunits of the PDH complex [17]. Thus, a major carbon flow from the cytoplasm to the mitochondrion in most eukaryotes is disconnected in the parasites, and alternative substrates such as amino acids must supplement intermediates in the TCA cycle [17,18]. As proposed for *Toxoplasma gondii* [14], branched-chain ketoacid dehydrogenase (BCKDH), a relative of PDH and 2-oxoglutarate dehydrogenase (2OGDH), could supply acetyl-CoA to the TCA cycle [19].

In contrast to *Plasmodium*, *Cryptosporidium* and the gregarines have a relatively simple parasitic strategy involving a single host and invasion of a single cell type, primarily intestinal epithelial cells. *C. parvum* and *C. hominis* lack TCA cycle enzymes except a membrane-bound malate-quinone oxidoreductase (MQO) (Fig. 2, Table S1) and their mitochondrion-derived organelle (mitosome) uses oxygen-sensitive pyruvate-$NADP^+$ oxidoreductase (PNO) in place of PDH. PNO consists of an *N*-terminal pyruvate-ferredoxin oxidoreductase (PFO) domain and a *C*-terminal NADPH-cytochrome P450 reductase

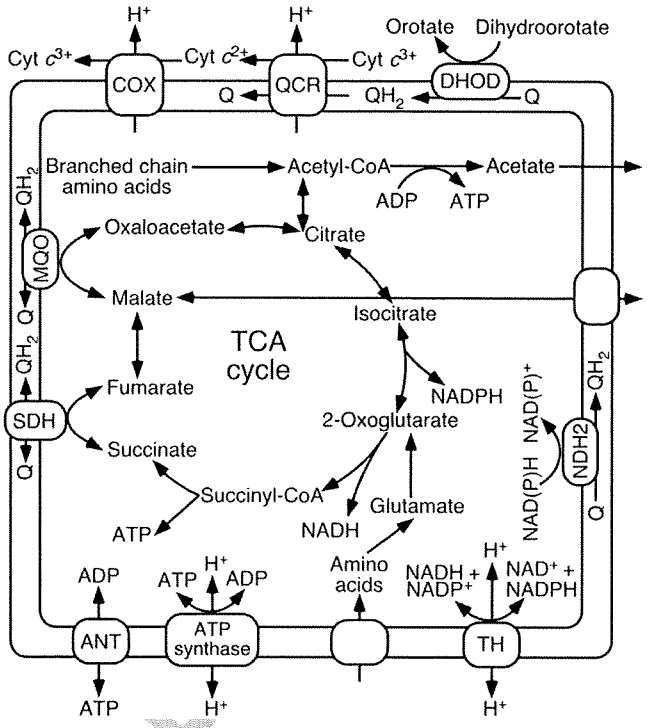

Fig. 1. Mitochondrial metabolic pathways in the human malaria parasite *P. falciparum*. Proton translocation machineries are F_oF_1-ATP synthase, ubiquinol-cytochrome *c* reductase (QCR), cytochrome *c* oxidase (COX), and NAD(P)-transhydrogenase (TH). Reduction of ubiquinone (Q) by alternative NADH dehydrogenase (NDH2), succinate dehydrogenase (SDH), malate-quinone oxidoreductase (MQO), and dihydroorotate dehydrogenase (DHOD) do not generate the proton-motive force. NAD-dependent malate dehydrogenase (MDH) and pyruvate dehydrogenase are located in the cytoplasm and apicoplast, respectively, and do not participate in TCA cycle. ATP produced by substrate-level phosphorylation by succinyl-CoA synthase (SCS) and acetyl-CoA synthase and by oxidative phosphorylation is exchanged with ADP in the cytoplasm *via* adenine nucleotide transporter (ANT). Expression levels of TCA cycle enzymes (fumarate hydratase, a flavoprotein subunit of SDH, SCS α subunit, aconitate hydratase, and citrate synthase), and α and β subunits of ATP synthase are increased in salivary gland sporozoites while the expression levels of glycolysis pathway enzymes (hexokinase, phosphoglycerate kinase, pyruvate kinase and 6-phosphofructokinase) are increased in asexual blood-stage trophozoites and schizonts (8; Lasonder, E., and Stunnenberg, H.G., personal communication). For the clarity, the outer membrane of the mitochondrion is not shown. In apicomplexan species, *Toxoplasma gondii* has a mitochondrial MDH [9] and *Babesia bovis* lacks TH [10].

domain and oxidizes pyruvate to acetyl-CoA [21–23]. On the basis of recent genome data and biochemical studies, we focus here on metabolic flow including electron and proton circuits and summarize unique properties of the modified TCA cycle and mitochondrial electron transfer chain in two pathogenic apicomplexan groups, *Plasmodium* and *Cryptosporidium*, and a related early branching group of dinoflagellates, *Perkinsus marinus*.

2. Human malaria parasite

Energy metabolism of *Plasmodium falciparum* is quite different from that of mammalian hosts. Intraerythrocytic stages of parasites have been considered for a long time to rely on incomplete oxidation of glucose, with secretion of end products such as lactate and pyruvate [24]. The mitochondrion can oxidize NADH, glycerol-3-phosphate, succinate, dihydroorotate, and amino acids, but it is essentially acristate and apparently lacks oxidative phosphorylation and a functional TCA cycle [6,7]. A lack of any severe phenotype in a gene disruptant for a flavoprotein subunit (SDH1, Fp) of succinate dehydrogenase complex (SDH, Complex II) in axenically cultured *P. falciparum* [25] suggests that the TCA cycle is not essential for energy metabolism in blood-stage parasites. Painter et al. [26] claimed that

Please cite this article as: Mogi T, Kita K, Diversity in mitochondrial metabolic pathways in parasitic protists *Plasmodium* and *Cryptosporidium*, Parasitol Int (2010), doi:10.1016/j.parint.2010.04.005

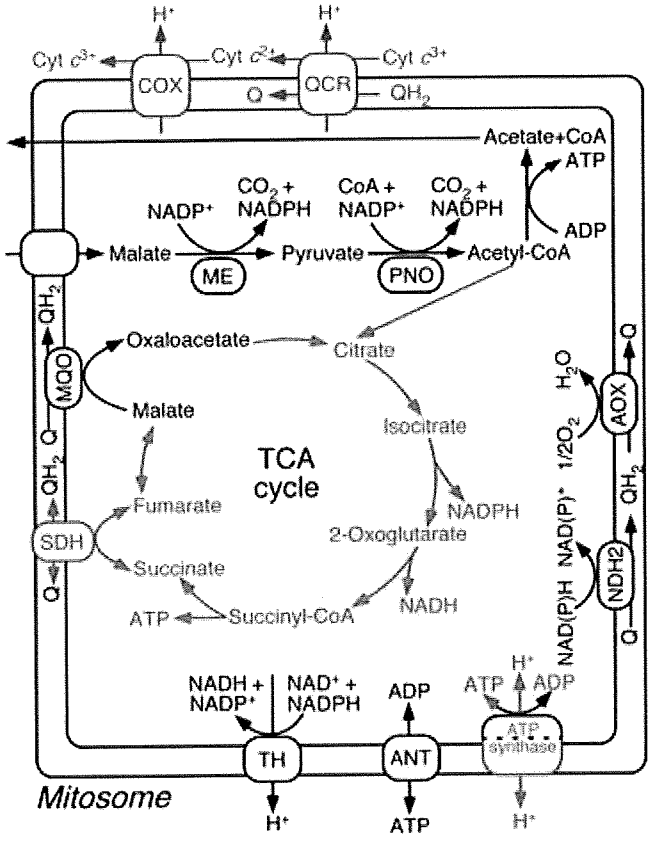

Fig. 2. Substrate-level phosphorylation in *C. parvum* mitosomes and oxidative phosphorylation catalyzed by *C. muris* and *P. marinus* mitosomes. Pathways and enzymes absent in *C. parvum* are shown in *red*. QCR and COX present only in *P. marinus* are shown in *blue*. Mitochondial targeting peptide score by TargetP 1.1 [20] of putative mitosome proteins (*C. muris*, *C. paruvum*) (Table S1) are TH βα-1 (0.085, 0.028) and βα-2 (0.079, 0.074), PNO (0.045, 0.051), NDH2 (0.389, 0.123), MQO (0.860, 0.837), AOX (0.639, 0.835), ANT (0.081, 0.146), ACS (0.135, 0.136), SDH1 [0.848, NA (not applicable)], SDH2 (0.191, NA), fumarate hydratase (0.571, NA), CS (0.111, NA), aconitate hydratase (0.203, NA), NADP-ICDH (0.076, NA), 2OGDH E1a (0.708, NA), SCS α (0.421, NA) and β (0.527, NA), and ATP synthase α (0.742, 0.265), β (0.573, 0.737), γ (0.789, NA), δ (0.896, NA), ε (0.320, NA), and *c* (0.646, NA). In the current genome data at NCBI, sequences of OSCP in the F_1 subdomain, subunits *a* and *b* in the F_o subdomain, and SDH3 and SDH4 of the SDH complex are not annotated or difficult to identify by BLAST search. *P. marinus* proteins except SDH3, SDH4, and subunits ε_m, *a*, *b*, and *d* of ATP synthase were all identified in the current database (http://www.tigr.org/tdb/e2k1/pmg/) (Table S1).

for the blood-stage *P. falciparum*, the mitochondrial respiratory chain is required for regeneration of an oxidized form of ubiquinone, which serves as the electron acceptor for type 2 dihydroorotate dehydrogenase, an essential enzyme for pyrimidine biosynthesis (Fig. 1). Thus, it is widely accepted that the majority of the parasite's ATP demand in the blood stages is met through glycolysis [7].

In the *Plasmodium* TCA cycle, isocitrate dehydrogenase (ICDH) is an NADP-dependent enzyme that can catalyze the reductive carboxylation of 2-oxoglutarate (2OG) [11,12,27,28] (Fig. 1). NAD-dependent malate dehydrogenase (MDH) in the mitochondrial matrix is replaced by MQO [29,30]. Apicomplexan MQO has been acquired by horizontal gene transfer from ε-proteobacteria [31,32] and energetically favors the oxidation of malate with ubiquinone [29]. Recent metabolomic studies on blood-stage *P. falciparum* suggest that when glutamine is supplied to the parasites, it is converted to 2OG, which is then metabolized to L-malate *via* the reductive carboxylation pathway though citrate and *via* the oxidative pathway through succinate (Olszewski K, Rabinowitz JD, and Llinás M, personal communication) (Fig. 1). Such a bifurcated pathway can produce ATP *via* substrate-level phosphorylation using succinyl-CoA synthase (SCS, succinate thiokinase) and acetyl-CoA synthase (ACS). To operate this unique pathway, NADPH needs to be reoxidized by NDH2 [33] or NAD(P) transhydrogenase (TH). Alternatively, if BCKDH [19,34,35] supplies acetyl-CoA to TCA cycle, substrates would be completely oxidized. Although there are variations in mitochondrial enzymes between *Plasmodium*, *Toxoplasma*, *Theileria*, and *Babesia* [19], similar mechanisms are operative in the apicomplexan species.

In blood-stage parasites, food vacuoles digest hemoglobin and other proteins into amino acids, potential precursors of TCA cycle intermediates. In the insect stages, the parasites can use amino acids in the mosquito hemolymph as carbon sources and carry out oxidative phosphorylation. Proteomic profiling studies have demonstrated metabolic readjustment from the glycolytic pathway in the asexual stage trophozoite and schizont to the TCA cycle in salivary gland sporozoites [9]. Transcriptome studies on blood-stage parasites isolated from patients showed that the parasites within human hosts take at least two physiological states [36–38]. One is related to ring forms and depends on glycolysis while the other is similar to gametocyes and sporozoites and depends on oxidative phosphorylation. Even though the expression levels of TCA cycle enzymes are low in the blood stages, the TCA cycle must produce some amount of succinyl-CoA for making 5-aminolevulinic acid (the first precursor of heme biosynthesis) *via* the oxidative pathway and may be essential at a specific physiological state. If the oxidative pathway functions in the reverse direction under hypoxic conditions, quinols produced by NDH2 (and MQO) can be reoxidized by the quinol-fumarate reductase activity of SDH.

3. Rodent malaria parasites

In the rodent parasite mitochondrion, succinate respiration, ATP synthesis, and the collapse of the mitochondrial membrane potential by atovaquone [39], a potent QCR inhibitor, suggest the presence of a functional oxidative phosphorylation system [40,41]. Biochemical studies indicate that both SDH and ATP synthase as well as NDH2, QCR, and COX must be fully functional [33,40–44], although the membrane anchor subunits of SDH (SDH3 (CybL) and SDH4 (CybS)) and of ATP synthase (subunits *a* and *b*) have not been identified in genome database because of their sequence diversity [11,12,45,46]. Recently, we showed in the rodent malaria parasite that *Plasmodium* SDH is a 130-kDa complex composed of four polypeptides [33]. Further, we identified all subunits of SDH (SDH1–SDH4) and ATP synthase [α, β, γ, OSCP (oligomycin-sensitivity conferring protein, δ), δ_m, ε_m, *d*, *a*, *b*, and *c*] in both human and rodent parasites [47]. Thus, malaria parasites can carry out oxidative phosphorylation in insect and mammalian stages through operating TCA cycle by using BCKDH and/or 2OG as an alternative means of entry into the TCA cycle.

4. *C. parvum*

C. parvum is a widespread intestinal intracellular parasite that causes diarrhea of mammals. Infection occurs following the ingestion of oocysts directly from the environment. A double-membrane mitochondrion-derived organelle (mitosome) lacking mtDNA was found to establish a membrane potential using a limited respiratory chain [48]. The eugregarine *Gregarina niphandrodes*, a close relative of *Cryptosporidium*, has a mitochondrion-like organelle with cristae but lacks the apicoplast [49], suggesting the loss of the plastid in the Apicomplexa following the divergence of gregarines and *Cryptosporidium*.

C. parvum and *C. hominis* genomes [15,16,21] encode mitochondrial PNO, NDH2, AOX, and TH (Fig. 2, Table S1). PNO has been originally found in the mitochondrion of the photosynthetic euglenozoan *Euglena gracilis* [21,23]. In contrast, Ctrnacta et al. [50] reported that *C. parvum* PNO was localized in the cytosol and crystalloid body, an enigmatic cryptosporidial organelle of unknown

Please cite this article as: Mogi T, Kita K, Diversity in mitochondrial metabolic pathways in parasitic protists *Plasmodium* and *Cryptosporidium*, Parasitol Int (2010), doi:10.1016/j.parint.2010.04.005

function [3]. Generation of membrane potential in the crystalloid body [50] indicates the similarity of this organelle to the mitosome.

Both *C. parvum* and *C. hominis* genomes [15,16] lack genes for all TCA cycle enzymes except MQO, and enzymes for oxidative phosphorylation [NDH1, QCR, COX and ATP synthase (except α and β subunits)] (Table S1). For ATP production, the parasites must rely on glycolysis or substrate-level phosphorylation in the mitosome. PNO oxidizes pyruvate and yields NADPH and acetyl-CoA, which can be used for ATP synthesis by ACS. Seeber et al. [19] suggested that NADPH does not contribute to energy production, but it can drive membrane-bound TH as a mitosomal proton pump (Fig. 2). NAD(P)H generated by malic enzyme (ME), PNO and/or TH is oxidized by NDH2 and resulting ubiquinols by AOX. Accordingly, membrane potential can be generated by a simple respiratory chain consisting of TH, NDH2 and AOX. Alternative scenario is the coupling of the internally bound AOX with the externally bound NDH2, which can reoxidize cytoplasmic NADH. Such scalar protolytic reactions can generate the proton-motive force. ATP and NADPH produced in the mitosome could be used for iron–sulfur cluster formation. However, predictions do not support the localization of *C. parvum* PNO (0.051 and 0.077, scores by TargetP [20] and MitoProt [51], respectively), ACS (0.135 and 0.031), and TH (0.028 and 0.584 in βα-1, 0.074 and 0.140 in βα-2) in the mitosome.

MQO and α and β subunits of ATP synthase encoded by *C. parvum* and *C. hominis* genomes have been frequently inferred to be active and to play a functional role in their mitosomes [19,52]. Unlike MQO from the rodent gastric parasite *Cryptosporidium muris* (537 amino acid residues), *C. hominis* MQO is truncated (313 *vs.* 527 amino acid residues in *C. parvum*) and lacks the FAD- and malate-binding sites [32,53,54]. ATP synthase α and β subunits of the human parasites both retain nucleotide-binding motifs, but the *C. hominis* subunits are again truncated (349 and 341 *vs.* 639 and 540 amino acid residues in *C. parvum*). Accordingly, *C. hominis* MQO and ATP synthase α and β subunits seem inactive and *C. parvum* proteins are likely intermediates in degeneration from *C. muris* sequences to *C. hominis* sequences. Further, it should be noted that *C. parvum* and *C. hominis* Coq2, Coq3 and Coq8 and *C. hominis* Coq4 and Coq7, which are involved in ubiquinone biosynthesis, are not well conserved. Thus, *C. parvum* and *C. hominis* MQO and ATP synthase α and β subunits could be relict proteins and their physiological roles and enzymatic activities as well as the presence of ubiquinone in the mitosome need to be biochemically examined in future studies.

5. *C. muris*

In contrast to the human intestinal parasites, genome data mining uncovered that the rodent gastric parasite *C. muris* has all TCA cycle enzymes including a functional MQO and SDH as well as ATP synthase (Fig. 2, Table S1). *C. muris* parasites are larger than *C. parvum* parasites, and *C. muris* mitosome has been recognized with its double-membrane envelope and tubular cristae [55]. In *C. muris* mitosome, acetyl-CoA produced by PNO can be fully oxidized by the canonical TCA cycle. NADPH produced by ME, PNO and ICDH could drive TH to generate a proton-motive force. It should be noted that in all apicomplexan species the α subunit of TH is fused to the C-terminus of the β subunit. NAD(P)H and ubiquinol produced by TH and/or TCA cycle enzymes are reoxidized by the *Cryptosporidium* respiratory chain consisting of NDH2 and AOX. To participate in TCA cycle, both NDH2 and MQO need to be bound at the matrix side of the inner membrane. The *N*-terminus sequences of *Cryptosporidium* iron-containing superoxide dismutase (SOD), adenine nucleotide transporter (ANT), NDH2, MQO, and AOX showed the distribution of hydrophobic and positively charged amino acid residues similar to those of *C. parvum* matrix proteins [56,57] (Fig. 3), indicating the presence of the mitochondrial targeting sequence. In contrast, PNO has distinct features in the *N*-terminal sequences [50]. Since PNO is essential for *C. muris* TCA cycle, *Cryptosporidium* PNO likely has an internal or alternative mitosome-targeting signal.

In conclusion, the *C. muris* mitosome has all TCA cycle enzymes and ATP synthase. Besides substrate-level phosphorylation by ACS and SCS, the *C. muris* mitosome can generate ATP *via* oxidative phosphorylation with the simplified respiratory chain. At this moment, it is difficult to decide whether *C. muris* mitosome should be assigned to the mitochondrion or not. The ongoing genome project on *C. muris* (http://msc.jcvi.org/c_muris/genbank_data.shtml) will provide clues for the presence or absence of the mitochondrial genome, and the membrane anchors of ATP synthase (subunits *a* and *b*) and SDH (SDH3 and SDH4). Proposed metabolic pathways of the *C. muris* mitosome invoked by our analysis now need experimental supports.

6. Ancestor of dinoflagellates and apicomplexans

Unique features of *Cryptosporidium* mitosomes are the presence of PNO and AOX and are shared only by the facultatively intracellular

```
C.parvum-CPN60      --MLLRSGINLYKSVEGSIGLRSAAIRFGMRYISSGKE*LS
C.muris-CPN60       -MSILSTLCNSTLNTLRSLKFTKIGCRYASTSKEIKFGNS
C.parvum-mtHSP70    -MSMIINSSFNG---VVNSSGIAARILKRSLPLVFSRY*MS
C.muris-mtHSP70     MFCTRYKNNSNFGNALKSISTFLIKTSSGILHRHIGTSAS
C.parvum-IscU       --MLQLRQLIDKRILIKKCVPICQRLFYS*DTVHDHFRNPR
C.muris-IscU        -MMIAVRNCITR--CKQHLSLIAQKAMYSEAVHDHFRNPR
C.parvum-IscS       --MIVHRYCRQWAPSVVRGIS-KLAFFSSMSSIAKKRPAY*
C.muris-IscS        ---MNMKTLPLGVSFISRRSKYLRSFSSKLKRQSIQRPLY
C.parvum-SOD        -MSIRFIFNNNSKKLVNKFCRL*SGMPFELPPLPYDKKAL
C.muris-SOD         -MS-RYITKYLLSQFLIKRAN-FSTMVFELPPLPYPKTAL
C.parvum-ANT        -ME-NKKEEKQNKK---KKNNFLTDFIVGGISATISKTAV
C.muris-ANT         -MT-SIKQNSEDVEFCSKFNSFALDFTTGGISAALSKTAV
C.parvum-NDH2       -MSNSEKNTSNIRTCSSVFAEDEKKNVSNTFSTITNKATS
C.muris-NDH2        -MKLLTLGLIDISPVFKRNMIFHLRWLSSSSVTCLKRYAE
C.parvum-MQO        -MLNLQRIMGRTCLRSSIINKKVISMSNSYLSRGLERRNI
C.muris-MQO         ----MLRKFVNREFLHISRSFYIGSILSNTRRLTSVKNTV
C.parvum-AOX        --MYYVRNLSNTNKLRYFYGRHLWLLSSKVNLNNLCSIVH
C.muris-AOX         -MNFQSNISRNIISSFNQLFFNCNYIKATNKCITTSRHIS
C.parvum-PNO        ---MGEKEIVDGCVAACHIAYACSEVAFTYPITPSSTISE
C.muris-PNO         ---MKS-EIVDGCVAACHIAYACSEVAFIYPITPSSSISE
```

Fig. 3. Multiple sequence alignment of the *N*-terminus sequences of *Cryptosporidium* mitosome enzymes. AOX, MQO and NDH2 are bound peripherally to the inner membranes while iron-containing SOD and ANT are a matrix protein and an intrinsic inner membrane protein, respectively. Hydrophobic and positively charged amino acid residues are shown in *orange* and *blue*, respectively. Sequences used are chaperonin 60 (CPN60), mitochondrial heat shock protein (mtHSP70), molecular scaffold protein for the formation of a transient FeS cluster (IscU), cysteine desulfurase (IscS), SOD, ANT, NDH2, MQO, AOX, and PNO of C. parvum and *C. muris*. Proposed cleavage sites in *P. parvum* CPN60, mtHSP70, IscU, IscS, and SOD [56,57] are indicated by *asterisks*. In case of CPN60, mtHSP70, and SOD, the sites are within the R2 motif, xRx(S/x) [58].

Please cite this article as: Mogi T, Kita K, Diversity in mitochondrial metabolic pathways in parasitic protists *Plasmodium* and *Cryptosporidium*, Parasitol Int (2010), doi:10.1016/j.parint.2010.04.005

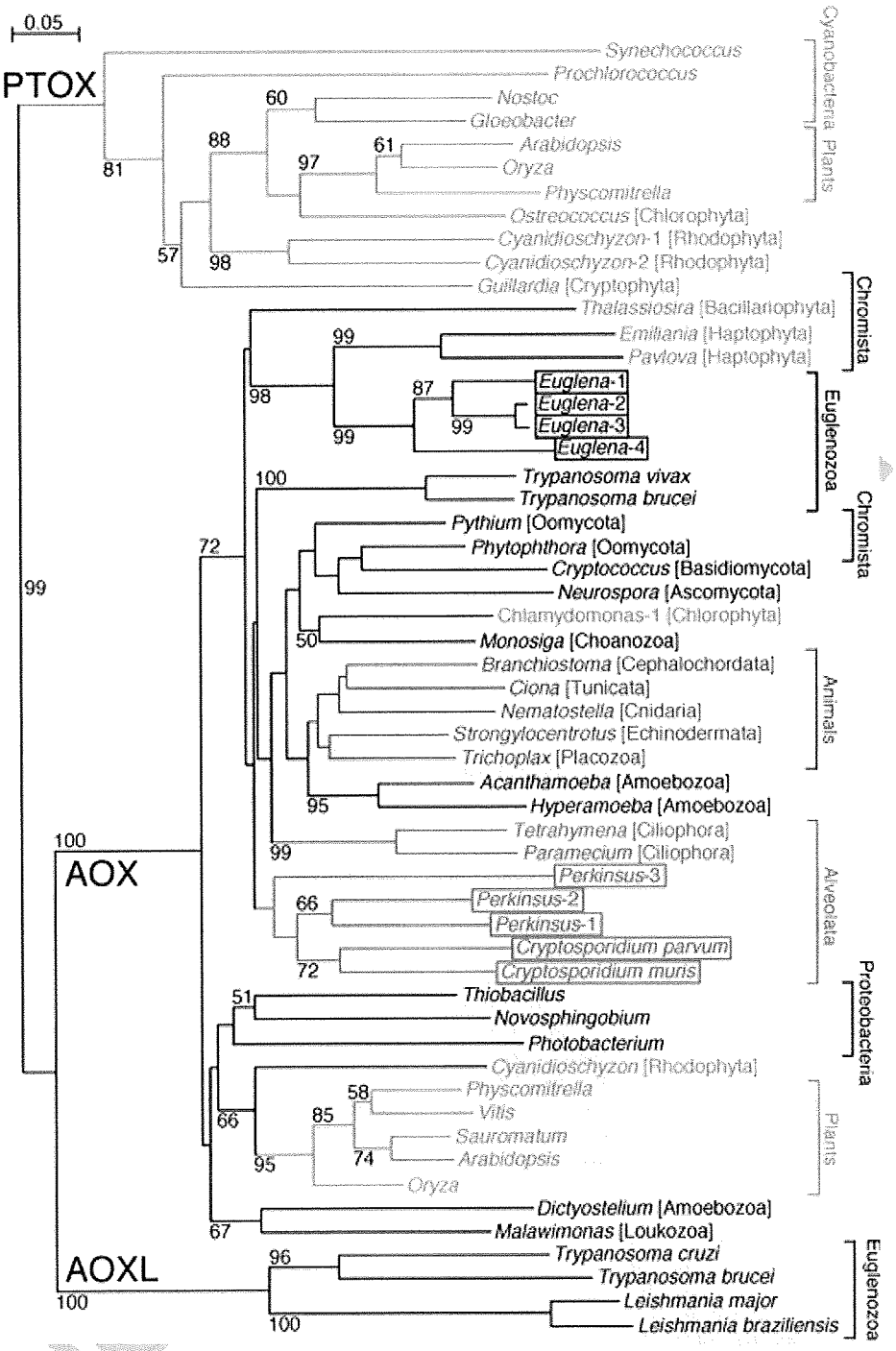

Fig. 4. Phylogenetic analysis of alternative oxidase (AOX), AOX-like proteins (AOXL), and plastid terminal oxidase (PTOX). AOX sequences used are: *C. muris*, XP_002141506; *C. parvum*, XP_626866; *P. marinus*, EEQ98001 (AOX1), EER20415 (AOX2), and EEQ98881 (AOX3); *E. gracilis*, EC681555 (AOX1), EC676833 (AOX2), EC679901 (AOX3), and EC682967 (AOX4); *Leishmania braziliensis*, XP_001569080 (AOXL); *Leishmania major*, XP_001687022 (AOXL); *Trypanosoma brucei*, XP_823198 (AOXL) and XP_822944 (AOX); *Trypanosoma cruzi*, XP_819840 (AOXL); *Trypanosoma vivax*, BAD11307 (AOX); *Paramecium tetraurelia*, XP_001459809; *Tetrahymena thermophila*, XP_001025570 (AOX2); *Acanthamoeba castellanii*, ABB04275 (AOXB); *Dictyostelium discoideum*, XP_641001; *Hyperamoeba dachnaya*, EC855215; *Malawimonas jakobiformis*, EC726821; *Monosiga brevicollis*, XP_001743500; *Pythium aphanidermatum*, CAE11918; *Phytophthora capsici*, FG051948; fungi [*Cryptococcus neoformans*, XP_566622 (AOX1); *Neurospora crassa*, XP_962086]; animals [*Branchiostoma floridae*, XP_002225713; *Ciona intestinalis*, FF738463; *Nematostella vectensis*, XP_001635929; *Strongylocentrotus purpuraus*, XP_785497; *Trichoplax adhaerens*, XP_002110128]; *Ostreococcus lucimarinus*, XP_001420304 (PTOX); *Cyanidioschyzon merolae*, CMI243C (PTOX1), CMI244C (PTOX2), and CMI072C; *Guillardia theta*, CAI77910 (PTOX); *Thalassiosira pseudonana*, XP_002294653; *Emiliania huxleyi*, GE163951; *Pavlova lutheri*, EC175359; *Chlamydomonas reinhardtii*, XP_001694605 (AOX1); plants [*Physcomitrella patens*, XP_001766430 (PTOX2), and XP_001774858; *Arabidopsis thaliana*, CAA06190 (PTOX), and NP_188876 (AOX1a); *Oryza sativa*, NP_001054199 (PTOX), and NP_001053759; *Sauromatum guttatum*, CAA78823; *Vitis vinifera*, XP_002262982]; cyanobacteria [*Synechococcus* sp. PCC9902, YP_376451 (PTOX); *Prochlorococcus marinus*, YP_396838 (PTOX); *Nostoc* PCC 7120, NP_486136 (PTOX); *Gloeobacter violaceus* PCC 7421, NP_923547 (PTOX)]; proteobacteria [*Thiobacillus denitrificans*, YP_315688; *Novosphingobium aromaticivorans*, YP_496850; *Photobacterium* SKA34, ZP_01159533]. *S. purpuratus* AOX (1014 residues) has a 700 amino acid residue *N*-terminus extension, which has the similarity to *Danio rerio* histone-lysine *N*-methyl transferase (XP_001920586, 39% identity) and vasopressin V2 receptor (residue 264 to 822 of XP_001346005, 39% identity). Sequences were obtained at NCBI except *C. merolae* (*Cyanidioschyzon merolae* genome project, http://merolae.biol.s.u-tokyo.ac.jp/). Bootstrap values greater than 50% are shown. Species which have PNO are boxed. GenBank accession nos. for PNO from *E. gracilis* and *Perkinsus marinus* are Q94IN5 and EER03433, respectively.

Please cite this article as: Mogi T, Kita K, Diversity in mitochondrial metabolic pathways in parasitic protists *Plasmodium* and *Cryptosporidium*, Parasitol Int (2010), doi:10.1016/j.parint.2010.04.005

oyster parasite *P. marinus* and the free-living, facultatively anaerobic phototroph *E. gracilis* (Fig. 4, Table S1). *P. marinus* is considered as one of the early diverging groups of the lineage leading to the dinoflagellates [59–61]. In contrast to alveolata AOX, euglenozoan AOX and AOX-like protein (AOXL), which lack a diiron-binding motif $(E{-}ExxH)_2$, are scattered within the phylogenetic tree, indicating the lateral gene transfer of AOX (*e.g.*, from Haptophyta to Euglenida or Euglenozoa). Likewise, euglenids may have acquired the PNO gene from the ancestor of the Apicomplexa. Other notable feature is the absence of mitochondrial PDH in euglenids and apicomplexan species. Upon the secondary endosymbiosis of a green alga in the former and a red alga in the latter, α-proteobacteria-derived nuclear PDH genes have been replaced with new coming algal PDH genes but algal PDHs have been redirected to transport to chloroplasts and apicoplasts, respectively. It is unclear whether all these events have occurred as parallel evolution in two lineages.

Sequence analysis at TIGR *P. marinus* Sequence Database (http://blast.jcvi.org/er-blast/index.cgi?project=pmg) and NCBI suggests that *P. marinus* mitochondrion lacks NDH1 like the apicomplexan species but retains all other respiratory complexes along with NDH2, MQO and ATP synthase, illustrating the similarity to *C. muris* mitosomes (Table S1). Analysis of the mitochondrial genome of the early branching dinoflagellate *Oxyrrhis marina* revealed that the genome contains only two protein coding genes, *cox1* and a *cob–cox3* fusion [62–64]. As demonstrated for the dinoflagellate *Alexandrium catenella*, *Perkinsus* QCR and COX must be catalytically functional [65]. It will be of interest to know how the *P. marinus* mitochondrial genome is organized [63].

7. Remodeling mitochondrial carbon and energy metabolism with gains and losses of enzymes

Organisms remodel existing enzymes and pathways for adaptation to new environments. For example, Cox1, the Cu_A domain of Cox2, and Cox3 of cytochrome *c* oxidase subunits have evolved from anaerobic denitrification enzymes, nitric oxide reductase NorB subunit, nitrous oxide reductase (NosZ), and NorE, respectively [66]. *Nyctotherus ovalis* is an anaerobic heterotrichous ciliate found in the hindgut of cockroaches and contains a mitochondrion-derived organelle, hydrogenosome [67–70]. Hydrogenosomes are surrounded by a double-membrane with cristae-like structures and contain a genome (~11 kb) [71,72]. *N. ovaris* hydrogenosome retains the oxidative half of TCA cycle (from 2OG to malate) and uses this pathway for anaerobic fumarate respiration [67] while the hydrogenosome of *Trichomonas vaginalis* (an anaerobic parasitic metamonad) lacks further fumarate hydratase and SDH and uses SCS for substrate-level phosophorylation [68] (Fig. S1, Table S2). In the hydrogenosome matrix, dioxygen molecules are detoxified by antioxidant enzymes, flavodiiron family NAD(P)H oxidase (FDP) [73–75], NADPH-quinone reductases (NQO1 and MdaB) [76,77], SOD, and thioredoxin peroxidase (TrxP) (Fig. S1). NDH1 is known to consist of 46 subunits in bovine mitochondria and 14 subunits (NuoA–NuoN) in bacteria while *T. vaginalis* hydrogenosome retains only two catalytic subunits, 24 kDa (NuoE) and 51 kDa (NuoF) [68,78,79]. The 24/51 kDa heterodimer appears to function as NADH-oxidizing subunits of bacterial NAD-reducing hydrogenase (*e.g.*, HoxUF of *Ralstonia eutropha*), and transfer electron to [Fe]-hydrogenase *via* ferredoxin (Fdx) (Fig. S1). Oxidation of protons in the hydrogenosome matrix to molecular hydrogen by [Fe]-hydrogenase could produce the proton-motive force (inside negative and alkaline) across the membrane. In the absence of ATP synthase and the respiratory chain, the hydrogenosome generates ATP by ACS and SCS (Fig. S1). Thus, in hydrogenosomes of the anaerobic parasitic protists, mitochondrial enzymes have been reorganized to oxygen-independent ATP generation systems.

In contrast to reductive evolution of NDH1 in *N. ovalis* and *T. vaginalis* [68,70,78,79], recent proteomic studies revealed the presence of a NDH1-like novel redox complex in *Trypanosoma brucei* [80,81]. *In silico* studies on *T. brucei* NDH1 identified five membrane-bound subunits and eighteen soluble subunits including two plant-specific subunits [82,83] (Table S2). Among them eight subunits are encoded by mitochondrial maxicircle DNA. Proteomic studies on *T. brucei* mitochondria revealed that a soluble NDH1 subcomplex contained 29 proteins including eleven NDH1 subunits, two each of SOD and NADPH-quinone reductases, adrenodoxin reductase, chaperone DnaJ, and twelve hypothetical proteins [80,81] (Table S2). In sum, native *T. brucei* NDH1 would consist of more than 42 proteins with a calculated total mass of 1769 kDa (24 NDH1 subunits, 831 kDa; 18 other proteins, 938 kDa). Blue-native PAGE analysis of NDH1 from the plant trypanosomatid *Phytomonas serpens* identified 2.2 and 0.7 MDa NADH dehydrogenase complexes containing at least two NDH1 subunits, 39 kDa and B14 (LYR) [84]. *P. serpens* NDH1 (subcomplex) showed rotenone-, and piericidin A-sensitive NADH-ubiquinone reductase activity although much less sensitive than mammalian enzymes [84]. However, analysis of *Trypanosoma cruzi* strain lacking mitochondrial *ND4*, *ND5* and *ND7* genes demonstrated that ND deletions did not affect mitochondrial membrane potential and H_2O_2 production [85], indicating that NDH1 is not significantly involved in energy transduction in *T. cruzi*. It should be noted that trypanosomatid 75 kDa (NuoG), one of the catalytic subunits, is truncated (34 kDa) [82] while B4 (~15 kDa protein) is a part of 77–83 kDa trypanosomatid subunits [84]. The presence of novel subunits in *T. brucei* NDH1 suggests that alternative functions of trypanosomatid NDH1 could be lipid biosynthesis [*i.e.*, *trans*-2-enoyl-CoA reductase-like proteins (NADPH-quinone reductases), acyl-CoA synthase] [80,81] or detoxification of dioxygen (*i.e.*, two SOD, two NADPH-quinone reductases, and one adrenodoxin reductase).

Apicomplexans are obligate intracellular parasites and occupy diverse niches [17]. During reductive evolution, the parasites remodeled their metabolic pathways by losing and gaining many enzymes [19]. In a common ancestor of apicomplexa and dinoflagellates, a loss of the membrane-bound NDH1 subunits encoded by mtDNA has eliminated NDH1, the largest respiratory complex (~0.5 MDa in bacteria and ~1 MDa in mitochondria) in the mitochondria. A complete loss of mtDNA in the lineage of *Cryptosporidium* [52] eliminated QCR and COX because of the lack of the mtDNA-encoded membrane-bound subunits, Cob (QCR) and Cox1 and Cox3 (COX). The human parasites *C. parvum* and *C. hominis* further lost TCA cycle enzymes and ATP synthase subunits (Fig. 2). Upon a loss of the mitochondrial PDH, the ancestor of the alveolates has acquired PNO and MQO, which are retained in the extant *Cryptosporidium* and *Perkinsus*, the early branching groups of apicomplexa and

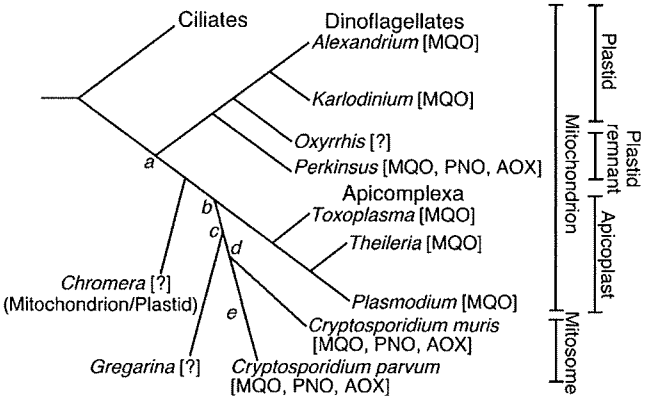

Fig. 5. Phylogeny of the Alveolata showing the loss and gain of mitochondrial enzymes. *a*, *b*, *c*, *d*, and *e* indicate a gain of MQO and PNO, a loss of NDH1 in the apicomplexan lineage, a loss of mtDNA and apicoplast in the gregarine/*Cryptosporidium* lineage, a loss of QCR and COX, and a loss of SDH and functional ATP synthase, respectively. *C. hominis*, a close relative of *C. parvum*, lacks PNO.

Please cite this article as: Mogi T, Kita K, Diversity in mitochondrial metabolic pathways in parasitic protists *Plasmodium* and *Cryptosporidium*, Parasitol Int (2010), doi:10.1016/j.parint.2010.04.005

dinoflagellates, respectively (Fig. 5). Other lineages like *Plasmodium* have established novel mechanisms for fueling TCA cycle (*i.e.* the use of BCKDH and/or 2OG as an alternative means of entry into TCA cycle). Throughout evolution, parasitic protists continue to remodel and use the mitochondrion-derived organelle and enzymes for aerobic or anaerobic oxidation of substrates and for energy production. Metabolic pathways in parasite mitochondria and mitosomes are varied largely from those of mammalian hosts and are the potential targets for new chemotherapeutics. We hope that extensive screening of chemical and natural compound libraries will identify specific and potent antibiotics targeting their specialized proteins with diversified sequences.

8. Uncited reference

[8]

Acknowledgements

This study was supported by a Grant-in-Aid for Scientific Research (20570124 to TM) and Creative Scientific Research (18GS0314 to KK) from the Japan Society for the Promotion of Science and for Scientific Research on Priority Areas (18073004 to KK) from the Ministry of Education, Culture, Sports, Science and Technology, Japan. We would like to thank Drs. M Llinás (Princeton University), L Lasonder and HE Stunnenberg (Radboud University Nijmegen) for the use of unpublished results and Dr. M Matsuzaki (University of Tokyo) and the anonymous referee for valuable comments. We would like to appreciate sequencing efforts by teams of the *Perkinsus marinus* genome project at the Institute for Genomic Research and of the *Cryptosporidium muris* genome sequence project at the J. Craig Venter Institute.

Appendix A. Supplementary data

Supplementary data associated with this article can be found, in the online version, at doi:10.1016/j.parint.2010.04.005.

References

[1] Leander BS. Marine gregarines: evolutionary prelude to the apicomplexan radiation? Trends Parasitol 2007;24:60–7.
[2] Ralph SA, van Dooren GG, Waller RF, Crawford MJ, Fraunholz MJ, Foth BJ, et al. Metabolic maps and functions of the *Plasmodium falciparum* apicoplast. Nature Rev Microbiol 2004;2:203–16.
[3] Keithly JS, Langreth SG, Buttle KF, Mannella CA. Electron tomographic and ultrastructural analysis of the *Cryptosporidium parvum* relict mitochondrion, its associated membranes, and organelles. J Eukaryot Microbiol 2005;52:132–40.
[4] Templeton TJ, Iyer LM, Anantharaman V, Enomoto S, Abrahante JE, Subramanian GM, et al. Comparative analysis of Apicomplexa and genomic diversity in eukaryotes. Genome Res 2004;14:1686–95.
[5] Henn MW, Schopf R, Maier WA, Seitz HM. The amino acid composition of *Anopheles stephensi* (Diptera: Culicidae) infected with *Nosema algerae* (Microsporida: Nosematidae). J Invertebrate Pathol 1998;71:42–7.
[6] Fry M, Beesley JE. Mitochondria of mammalian *Plasmodium* spp. Parasitology 1991;102:17–26.
[7] van Dooren GG, Stimmler LM, McFadden GI. Metabolic maps and functions of the *Plasmodium* mitochondrion. FEMS Microbiol Rev 2006;30:596–630.
[8] Lasonder E, Janse CJ, van Gemert G, Mair GR, Vermunt AMW, Douradinha BG, et al. Proteomic profiling of *Plasmodium* sporozoite maturation identifies new proteins essential for parasite development and infectivity. PLoS Pathogens 2008;4: e1000195.
[9] Fleige T, Pfa N, Gross U, Bohne W. Localisation of gluconeogenesis and tricarboxylic acid (TCA)-cycle enzymes and first functional analysis of the TCA cycle in *Toxoplasma gondii*. Int J Parasitol 2008;38:1121–32.
[10] Brayton KA, Lau AOT, Herndon DR, Hannick L, Kappmeyer LS, Berens SJ, et al. Genome sequence of *Babesia bovis* and comparative analysis of Apicomplexan hemoprotozoa. PLoS Pathogens 2007;3:1401–13.
[11] Gardner MJ, Hall N, Fung E, White O, Berriman M, Hyman RW, et al. Genome sequence of the human malaria parasite *Plasmodium falciparum*. Nature 2002;419: 498–511.
[12] Carlton JM, Angiuoli SV, Suh BB, Kooij TW, Pertea M, Silva JC, et al. Genome sequence and comparative analysis of the model rodent malaria parasite *Plasmodium yoelii yoelii*. Nature 2002;419:512–9.
[13] Foth BJ, Stimmler LM, Handman E, Crabb BS, Hodder AN, McFadden GI. The malaria parasite *Plasmodium falciparum* has only one pyruvate dehydrogenase complex, which is located in the apicoplast. Mol Microbiol 2005;55:39–53.
[14] Fleige T, Fischer K, Ferguson DJ, Gross U, Bohne W. Carbohydrate metabolism in the *Toxoplasma gondii* apicoplast: localization of three glycolytic isoenzymes, the single pyruvate dehydrogenase complex, and a plastid phosphate translocator. Eukaryot Cell 2007;6:984–96.
[15] Abrahamsen MS, Templeton TJ, Enomoto S, Abrahante JE, Zhu G, Lancto CA, et al. Complete genome sequence of the Apicomplexan, *Cryptosporidium parvum*. Science 2004;304:441–5.
[16] Xu P, Widmer G, Wang Y, Ozaki LS, Alves JM, Serrano MG, et al. The genome of *Cryptosporidium hominis*. Nature 2004;431:1107–12.
[17] Gardner MJ, Bishop R, Shah T, de Villiers EP, Carlton JM, Hall N, et al. Genome sequence of *Theileria parva*, a bovine pathogen that transforms lymphocytes. Science 2005;309:134–7.
[18] Teng R, Junankar PR, Bubb WA, Rae C, Mercier P, Kirk K. Metabolite profiling of the intraerythrocytic malaria parasite *Plasmodium falciparum* by ^{1}H NMR spectroscopy. NMR Biomed 2009;22:292–302.
[19] Seeber F, Limenitakis J, Soldati-Favre D. Apicomplexan mitochondrial metabolism: a story of gains, losses and retentions. Trends Parasitol 2008;24:468–78.
[20] Emanuelsson O, Nielsen H, Brunak S, von Heijne G. Predicting subcellular localization of proteins based on their N-terminal amino acid sequence. J Mol Biol 2000;300:1005–16.
[21] Rotte C, Stejskal F, Zhu G, Keithly JS, Martin W. Pyruvate:NADP oxidoreductase from the mitochondrion of *Euglena gracilis* and from the Apicomplexan *Cryptosporidium parvum*: a biochemical relic linking pyruvate metabolism in mitochondriate and amitochondriate protists. Mol Biol Evol 2001;18:710–20.
[22] Inui H, Ono K, Miyatake K, Nakano Y, Kitaoka S. Purification and characterization of pyruvate:NADP^{+} oxidoreductase in *Euglena gracilis*. J Biol Chem 1987;262:9130–5.
[23] Nakazawa M, Inui H, Yamaji R, Yamamoto T, Takenaka S, Ueda M, et al. The origin of pyruvate:NADP^{+} oxidoreductase in mitochondria of *Euglena gracilis*. FEBS Lett 2000;479:155–6.
[24] Sherman IW. Carbohydrate metabolism of asexual stages. In: Sherman IW, editor. Malaria, parasite biology, pathogenesis and protection. Washington, DC: ASM Press; 1998. p. 135–43.
[25] Tanaka T. Gene disruption of the flavoprotein subunit in succinate-ubiquinone reductase from *Plasmodium falciparum*. PhD Thesis, Univ. of Tokyo, 2008.
[26] Painter HJ, Morrisey JM, Mather MW, Vaidya AB. Specific role of mitochondrial electron transport in blood-stage *Plasmodium falciparum*. Nature 2007;446:88–91.
[27] Wrenger C, Muller S. Isocitrate dehydrogenase of *Plasmodium falciparum*. Eur J Biochem 2003;270:1775–83.
[28] Yoo H, Antoniewicz MR, Stephanopoulos G, Kelleher JK. Quantifying reductive carboxylation flux of glutamine to lipid in a brown adipocyte cell line. J Biol Chem 2008;283:20621–7.
[29] Molenaar D, van der Rest ME, Petrovic S. Biochemical and genetic characterization of the membrane-associated malate dehydrogenase (acceptor) from *Corynebacterium glutamicum*. Eur J Biochem 1998;254:395–403.
[30] Kather B, Stingl K, van der Rest ME, Altendorf K, Molenaar D. Another unusual type of citric acid cycle enzyme in *Helicobacter pylori*: the malate:quinone oxidoreductase. J Bacteriol 2000;182:3204–9.
[31] Nosenko T, Bhattacharya D. Horizontal gene transfer in chromalveolates. BMC Evol Biol 2007;7:173.
[32] Mogi T, Murase Y, Mori M, Shiomi K, Ōmura S, Paranagama MP, Kita K. (in press) Polymyxin B identified as an inhibitor of alternative NADH dehydrogenase and malate: quinone oxidoreductase from the Gram-positive bacterium *Mycobacterium smegmatis*. J Biochem 2009;146: (doi:10.1093/jb/mvp096). Q2
[33] Kawahara K, Mogi T, Tanaka TQ, Hata M, Miyoshi H, Kita K. Mitochondrial dehydrogenases in the aerobic respiratory chain of the rodent malaria parasite *Plasmodium yoelii yoelii*. J Biochem 2009;145:229–37.
[34] Heath C, Posner MG, Aass HC, Upadhyay A, Scott DJ, Hough DW, et al. The 2-oxoacid dehydrogenase multi-enzyme complex of the archaeon *Thermoplasma acidophilum*-recombinant expression, assembly and characterization. FEBS J 2007;274:5406–15.
[35] Pettit FH, Yeaman SJ, Reed LJ. Purification and characterization of branched chain alpha-keto acid dehydrogenase complex of bovine kidney. Proc Natl Acad Sci USA 1978;75:4881–5.
[36] Daily JP, Scanfeld D, Pochet N, Roch KL, Plouffe D, Kamel M, et al. Distinct physiological states of *Plasmodium falciparum* in malaria-infected patients. Nature 2007;450:1091–5.
[37] Lovegrove FE, Peña-Castillo L, Liles WC, Hughes TR, Kain KC. *Plasmodium falciparum* shows transcriptional versatility within the human host. Trends Parasitol 2008;24:288–91.
[38] LeRoux M, Lakshmanan V, Daily JP. *Plasmodium falciparum* biology:analysis of *in vitro* versus *in vivo* growth conditions. Trends Parasitol 2009;25:474–81.
[39] Srivastava IK, Rottenberg H, Vaidya AB. Atovaquone, a broad spectrum antiparasitic drug, collapses mitochondrial membrane potential in malarial parasite. J Biol Chem 1997;272:3961–6.
[40] Uyemura SA, Luo S, Vieira M, Moreno SN, Docampo R. Oxidative phosphorylation and rotenone-insensitive malate- and NADH-quinone oxidoreductases in *Plasmodium yoelii yoelii* mitochondria in situ. J Biol Chem 2004;279:385–93.
[41] Uyemura SA, Luo S, Moreno SNJ, Docampo R. Oxidative phosphorylation, Ca^{2+} transport, and fatty acid-induced uncoupling in malaria parasites mitochondria. J Biol Chem 2000;275:9709–15.
[42] Biagini GA, Viriyavejakul P, O'Neill PM, Bray PG, Ward SA. Functional characterization and target validation of alternative Complex I of *Plasmodium falciparum* mitochondria. Antimicrob Agents Chemother 2006;50:1841–51.

Please cite this article as: Mogi T, Kita K, Diversity in mitochondrial metabolic pathways in parasitic protists *Plasmodium* and *Cryptosporidium*, Parasitol Int (2010), doi:10.1016/j.parint.2010.04.005

[43] Takashima E, Takamiya S, Takeo S, Mi-ichi F, Amino H, Kita K. Isolation of mitochondria from *Plasmodium falciparum* showing dihydroorotate dependent respiration. Parasitol Int 2001;50:273–8.
[44] Dong CK, Patel V, Yang JC, Dvorin JD, Duraisingh MT, Clardy J, et al. Type II NADH dehydrogenase of the respiratory chain of *Plasmodium falciparum* and its inhibitors. Bioorg Medicin Chem Lett 2009;19:972–5.
[45] Vaidya AB, Mather MWA. Post-genomic view of the mitochondrion in malaria parasites. Curr Top Microbiol Immunol 2005;295:233–50.
[46] Vaidya AB, Mather MW. Mitochondrial evolution and functions in malaria parasites. Annu Rev Microbiol 2009;56:221–31.
[47] Mogi T, Kita K. Identification of mitochondrial Complex II subunits SDH3 and SDH4 and ATP synthase subunits *a* and *b* in *Plasmodium* spp. Mitochondrion. in press.
[48] Henriquez FL, Richards TA, Roberts F, McLeod R, Roberts CW. The unusual mitochondrial compartment of *Cryptosporidium parvum*. Trends Parasitol 2005;21:68–74.
[49] Toso MC, Omoto CK. *Gregarina niphandrodes* may lack both a plastid genome and organelle. J Eukaryot Microbiol 2007;54:66–72.
[50] Ctrnacta V, Ault JG, Stejskal F, Keithly JS. Localization of pyruvate:NADP$^+$ oxidoreductase in sporozoites of *Cryptosporidium parvum*. J Eukaryot Microbiol 2006;53:225–31.
[51] Claros MG, Vincens P. Computational method to predict mitochondrially imported proteins and their targeting sequences. Eur J Biochem 1996;241:779–86.
[52] Keithly JS. The mitochondrion-related organelle of *Cryptosporidium parvum*. In: Tachezy J, editor. Hydrogenosomes and mitosomes: mitochondria of anaerobic eukaryotes. Microbiology monographHeidelberg: Springer; 2008. p. 231–53.
[53] McKie JH, Douglas KT. Evidence for gene duplication forming similar binding folds for NAD(P)H and FAD in pyridine nucleotide-dependent flavoenzymes. FEBS Lett 1991;279:5–8.
[54] Chan M, Sim TS. Functional characterization of an alternative [lactate dehydrogenase-like] malate dehydrogenase in *Plasmodium falciparum*. Parasitol Res 2004;92:43–7.
[55] Uni S, Iseki M, Maekawa T, Moriya K, Takada S. Ultrastructure of *Cryptosporidium muris* (strain RN 66) parasitizing the murine stomach. Parasitol Res 1987;74: 123–32.
[56] Dyall SD, Dolexal P. Protein import into hydrogenosomes and mitosomes. In: Tachezy J, editor. Hydrogenosomes and mitosomes: mitochondria of anaerobic eukaryotes. Microbiology monographHeidelberg: Springer; 2008. p. 21–73.
[57] Kang J, Cheun H, Kim J, Moon S, Park S, Kim T, et al. Identification and characterization of a mitochondrial iron-superoxide dismutase of *Cryptosporidium parvum*. Parasitol Res 2008;103:787–95.
[58] Gavel Y, von Heijne G. Cleavage-site motifs in mitochondrial targeting peptides. Protein Eng 1990;4:33–7.
[59] Saldarriaga JF, McEwan ML, Fast NM, Taylor FJR, Keeling PJ. Multiple protein phylogenies show that *Oxyhrris marina* and *Perkinsus marinus* are early branches of the dinoflagellate lineage. Int J System Evol Microbiol 2003;53:355–65.
[60] Keeling PJ. Chromoalveolates and the evolution of plastids by secondary endosymbiosis. J Eukaryot Microbiol 2009;56:1–8.
[61] Reeb VC, Peglar MT, Yoon HS, Bai JR, Wu M, Shiu P, et al. Interrelationships of chromoalveolates with a broadly sampled tree of photosynthetic protists. Mol Phylogenet Evol 2009;53:202–11.
[62] Slamovits CH, Saldarriaga JF, Larocque A, Keeling PJ. The highly reduced and fragmented mitochondrial genome of the early-branching dinoflagellate *Oxyrrhis marina* shares characteristics with both apicomplexan and dinoflagellate mitochondrial genomes. J Mol Biol 2007;372:356–68.
[63] Nash EA, Nisbet RER, Barbrook AC, Howe CJ. Dinoflagellates: a mitochondrial genome all at sea. Trends Genetics 2008;24:328–35.
[64] Waller RF, Jackson CJ. Dinoflagellate mitochondrial genomes: stretching the rules of molecular biology. BioEssays 2009;31:237–45.
[65] Kamikawa R, Nishimura H, Sako Y. Analysis of the mitochondrial genome, transcripts, and electron transport activity in the dinoflagellate *Alexandrium catenella* (Gonyaulacales, Dinophyceae). Phycol Res 2009;57:1–11.
[66] Saraste M, Castresana J. Cytochrome oxidase evolved by tinkering with denitrification enzymes. FEBS Lett 1994;341:1–4.
[67] Hackstein JHP, de Graaf RM, van Hellemond JP, Tielens AGM. Hydrogenosomes of anaerobic ciliates. In: Tachezy J, editor. Hydrogenosomes and mitosomes: mitochondria of anaerobic eukaryotes. Microbiology monographHeidelberg: Springer; 2008. p. 97–112.
[68] Hrdy I, Tachezy Müller M. Metabolism of *Trichomonas* hydrogenosomes. In: Tachezy J, editor. Hydrogenosomes and mitosomes: mitochondria of anaerobic eukaryotes. Microbiology monographHeidelberg: Springer; 2008. p. 113–45.
[69] van Dooren GG, Marti M, Tonkin CJ, Stimmler LM, Cowman AF, McFadden GI. Development of the endoplasmic reticulum, mitochondrion and apicoplast during the asexual life cycle of *Plasmodium falciparum*. Mol Microbiol 2005;57:405–19.
[70] Boxma B, de Graaf RM, van der Staay GWM, van Alen TA, Ricard G, Gabaldón T, et al. An anaerobic mitochondrion that produces hydrogen. Nature 2005;434:74–9.
[71] Akhmanova A, Voncken F, van Alen T, van Hoek A, Boxma B, Vogels G, et al. A hydrogenosome with a genome. Nature 1998;396:527–8.
[72] Martin WF, Müller M. Origin of mitochondria and hydrogenosomes. Berlin: Springer; 2007.
[73] Matteo AD, Scandurra FM, Testa F, Forte E, Sarti P, Brunori M, et al. The O_2-scavenging flavodiiron protein in the human parasite *Giardia intestinalis*. J Biol Chem 2008;283:4061–8.
[74] Vicente JB, Testa F, Mastronicola D, Forte E, Sarti P, Teixeira M, et al. Redox properties of the oxygen-detoxifying flavodiiron protein from the human parasite *Giardia intestinalis*. Arch Biochem Biophys 2009;488:9–13.
[75] Smutná T, Gonçalves VL, Saraiva LM, Tachezy J, Teixeira M, Hrdý I. Flavodiiron protein from *Trichomonas vaginalis* hydrogenosomes: the terminal oxygen reductase. Eukaryot Cell 2009;8:47–55.
[76] Cadenas E. Antioxidant and prooxidant functions of DT-diaphorase in quinone metabolism. Biochem Phrmacol 1995;49:127–40.
[77] Wang G, Robert J, Maier RJ. An NADPH quinone reductase of *Helicobacter pylori* plays an important role in oxidative stress resistance and host colonization. Infect Immun 2004;72:1391–6.
[78] Hrdy I, Hirt RP, Dolezal P, Bardonová L, Foster PG, Tachezy J, et al. *Trichomonas* hydrogenosomes contain the NADH dehydrogenase module of mitochondrial Complex I. Nature 2004;432:618–22.
[79] Dyall SD, Yan W, Delgadillo-Correa MG, Lunceford A, Loo JA, Clarke CF, et al. Non-mitochondrial Complex I proteins in a hydrogenosomal oxidoreductase complex. Nature 2004;431:1103–7.
[80] Panigrahi AK, Zíková A, Dalley RA, Acestor N, Ogata Y, Anupama A, et al. Mitochondrial complexes in *Trypanosoma brucei*. A novel complex and a unique oxidoreductase complex. Mol Cell Proteomics 2008;7:534–45.
[81] Panigrahi AK, Ogata Y, Zíková A, Anupama A, Dalley RA, Acestor N, et al. A comprehensive analysis of *Trypanosoma brucei* mitochondrial proteome. Proteomics 2009;9:434–50.
[82] Opperdoes FR, Michels PAM. Complex I of Trypanosomatidae: does it exist? Trends Parasitol 2008;24:310–7.
[83] Kannan S, Burger G. Unassigned MURF1 of kinetoplastids codes for NADH dehydrogenase subunit 2. BMC Genomics 2008;9:455.
[84] Cermáková P, Verner Z, Man P, Lukes J, Horáth A. Characterization of the NADH: ubiquinone oxidoreductase (Complex I) in the trypanosomatid *Phytomonas serpens* (Kinetoplastida). FEBS J 2004;274:3150–8.
[85] Carranza JC, Kowaltowski AJ, Mendonça MAG, de Oliveira TC, Gadelha FR, Zingales B. Mitochondrial bioenergetics and redox state are unaltered in *Trypanosoma cruzi* isolates with compromised mitochondrial Complex I subunit genes. J Bioenerg Biomembr 2009;41:299–308.

Please cite this article as: Mogi T, Kita K, Diversity in mitochondrial metabolic pathways in parasitic protists *Plasmodium* and *Cryptosporidium*, Parasitol Int (2010), doi:10.1016/j.parint.2010.04.005

J|A|C|S COMMUNICATIONS

Published on Web 03/18/2009

Covalent Protein Labeling Based on Noncatalytic β-Lactamase and a Designed FRET Substrate

Shin Mizukami, Shuji Watanabe, Yuichiro Hori, and Kazuya Kikuchi*

Graduate School of Engineering, Osaka University, 2-1 Yamadaoka, Suita, Osaka 565-0871, Japan

Received October 20, 2008; E-mail: kkikuchi@mls.eng.osaka-u.ac.jp

Fluorescence microscopy is one of the most common techniques employed in the field of life science. With the rapid progress that has been achieved with regard to optical systems, fluorescent proteins (FPs) have acquired important roles for fluorescence microscopy experiments. In order to visualize the localization and behavior of particular proteins of interest, FPs such as green fluorescent protein (GFP) have conventionally been used.[1] More recently, techniques for labeling proteins with small molecules have attracted the attention of many life scientists because they can extend the range of natural FPs, for example, by incorporating near-infrared fluorescent dyes, MRI contrast agents, or biofunctional molecules such as biotin. Several approaches for modifying proteins with small molecules have been commercialized, including methods based on the tetracysteine tag,[2] HaloTag,[3] and SNAP-tag.[4] Other protein labeling methods involving the use of biotin ligase,[5] transglutaminase,[6] hexahistidine,[7] tetra-aspartic acid,[8] etc. have also been reported. Among the abovementioned labeling methods, only the tetracysteine tag exhibits fluorogenic properties. In the other labeling methods, it is necessary to wash the treated cells prior to microscopic measurements to eliminate background fluorescence. Thus, new labeling techniques that satisfy the dual criteria of specificity and fluorogenicity are desirable.

In this paper, we report a specific protein labeling system with an off-on fluorescence switch. It involves covalent modification of a genetically engineered hydrolytic enzyme with a rationally designed fluorogenic probe that exploits the principle of fluorescence resonance energy transfer (FRET). Using this system, we can achieve specific and fluorogenic protein labeling under physiological conditions.

First, we designed the tag protein. Plant or bacterial proteins are preferably used to achieve bioorthogonal labeling in mammalian cells. We focused on β-lactamase as the candidate tag because β-lactamases are small bacterial enzymes that hydrolyze antibiotics containing a β-lactam structure and have no endogenous counterpart among eukaryotic cells.[9] β-Lactamase has been widely used as a reporter enzyme for examining gene expression in living mammalian cells.[10] Class A β-lactamases such as the 29 kDa TEM-1[11] have been extensively investigated with regard to their structures, enzyme reaction kinetics, substrate specificity, inhibitors, etc.[12] The reaction of TEM-1 with β-lactams involves acylation and deacylation steps (Scheme 1). In the acylation step, Ser70 attacks the amide bond of the β-lactam ring to form an intermediate acyl-enzyme complex (ES*). In the deacylation step, an activated water molecule hydrolyzes the ester bond of the intermediate to yield the product. Previous studies have shown that Glu166 is essential for the deacylation step[13] and that the E166N mutant of TEM-1 (^{E166N}TEM) accumulates the acyl-enzyme intermediate by markedly slowing deacylation (k_3) relative to acylation (k_2).[14] We hoped to exploit the properties of the ^{E166N}TEM mutant to covalently attach a fluorescent substrate to β-lactamase.

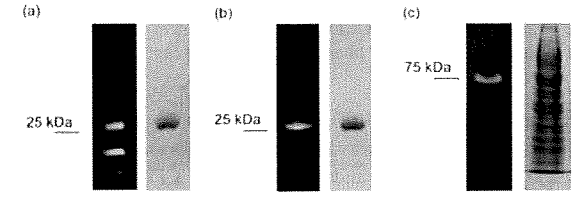

Figure 1. (a, b) Fluorescence (left) and CBB-stained (right) gel images of ^{E166N}TEM after incubation with (a) CA and (b) CCD. (c) Fluorescence and CBB-stained gel image of MBP-^{E166N}TEM mixed with HEK293T cell lysate after incubation with CCD.

Scheme 1. Mechanism of β-Lactam Cleavage by Class A β-Lactamases; (E) Enzyme, (S) Substrate, and (P) Product

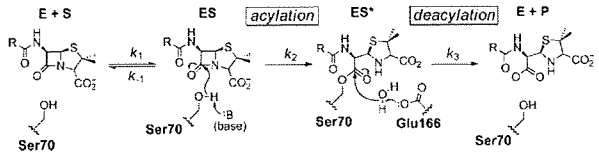

Scheme 2. Structures and Labeling Mechanisms of the Fluorescent Probes (a) CA and (b) CCD

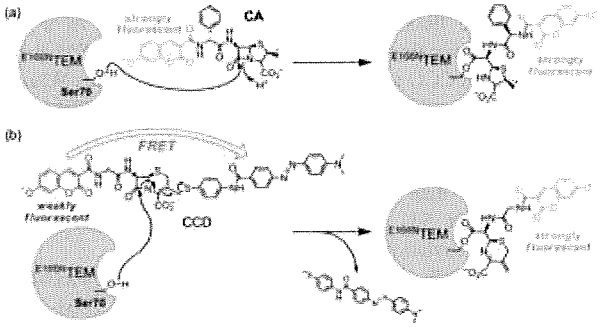

To investigate the feasibility of fluorescently labeling ^{E166N}TEM under physiological conditions, we designed and synthesized a penicillin-based fluorescent probe, coumarinyl ampicillin (CA). The labeling scheme is illustrated in Scheme 2a. Since CA contains 7-hydroxycoumarin, successfully labeled ^{E166N}TEM should exhibit cyan fluorescence. ^{E166N}TEM was incubated with CA in 10 mM Tris-HCl buffer (pH 7.0) at 25 °C, and protein labeling was assessed by SDS-PAGE. Fluorescent proteins were detected by irradiating the gels with UV light at 365 nm. When purified ^{E166N}TEM was mixed with CA, a protein band of ~29 kDa was observed that exhibited cyan fluorescence (Figure 1a); Coomassie Brilliant Blue (CBB) staining confirmed that this band corresponded to ^{E166N}TEM. In contrast, when wild-type (WT) TEM-1 was incubated with CA, no cyan fluorescence was seen (Figure S1a). Although CA successfully labels ^{E166N}TEM, other fluorescent bands were also observed on the gel. Since these bands were also seen when only

10.1021/ja8082285 CCC: $40.75

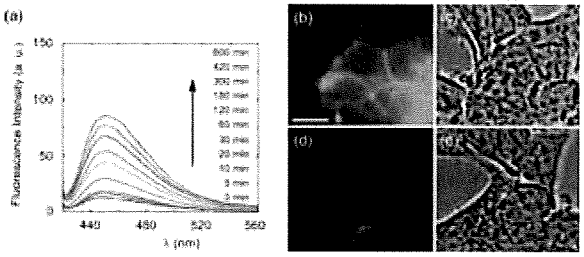

Figure 2. (a) Time-dependent emission spectra (λ_{ex} = 410 nm) of CCD (1 μM) in the presence of ^{E166N}TEM in 100 mM HEPES buffer (pH 7.4) containing 0.1% DMSO at 25 °C. (b–e) Optical microscopic images of CCD-labeled HEK293T cells expressing ^{E166N}TEM-EGFR (b,c) and EGFR (d,e), labeled with 5 μM CCD. (b,d) Fluorescence microscopic images, excitation at 410 nm. (c,e) phase contrast microscopic images. Scale bar: 10 μm.

CA was electrophoresed (Figure S2), a washing procedure should be performed before observation under a fluorescence microscope.

Next, we designed and synthesized CCD (Scheme 2b), a fluorescence off–on labeling probe. This molecule has three main components: 7-hydroxycoumarin, cephalosporin, and 4-(4′-dimethylaminophenylazo)benzoic acid (DABCYL). Since the absorption spectrum of DABCYL substantially overlaps with the emission spectrum of 7-hydroxycoumarin, the fluorescence of CCD would be expected to be largely quenched by intramolecular FRET from coumarin to DABCYL. Based on related probes of β-lactamase activity,[10] cleavage of the β-lactam of CCD by ^{E166N}TEM should result in covalent attachment of the coumarin to the protein with concomitant release of the DABCYL moiety as shown in Scheme 2b. After loss of the DABCYL group, the cyan fluorescence of coumarin should be restored by cancelation of FRET.

The fluorescence spectrum of CCD confirmed that the coumarin fluorescence was almost completely quenched because of FRET. The fluorescence quantum yield of CCD was 0.006, which is much lower than that of CA (Φ = 0.40). When CCD was incubated with ^{E166N}TEM, the fluorescence increased considerably in a time-dependent manner (Figure 2a). This indicates that ^{E166N}TEM cleaved the β-lactam of CCD and eliminated the DABCYL group. When the DABCYL group was completely eliminated by WT TEM-1, the fluorescence signal increased approximately 30-fold. The apparent rate of reaction between CCD and ^{E166N}TEM was approximately 80-fold slower than that of the reaction between CCD and WT TEM-1 (Figure S3), probably because the mutation at E166 decreases the acylation rate (k_2) somewhat.[15]

CCD specifically labels ^{E166N}TEM, as demonstrated by incubation of the probe molecule with both ^{E166N}TEM and WT TEM-1 in 10 mM Tris-HCl buffer (pH 7.0) at 25 °C, followed by SDS-PAGE analysis. As shown in Figure 1b, only the band corresponding to ^{E166N}TEM exhibited cyan fluorescence; no fluorescence was associated with WT TEM-1 (Figure S1b). In contrast to CA, unreacted CCD yielded considerably weaker fluorescence on the gel. In MALDI-TOF MS analyses of the samples, the molecular mass peak for the protein–probe adduct was only detected when ^{E166N}TEM was incubated with CCD (Figure S4).

This system can therefore be used to label target proteins in a biological medium. For example, we fused ^{E166N}TEM to maltose binding protein (MBP, 42 kDa), mixed the purified MBP–^{E166N}TEM construct with HEK293T cell lysate, and incubated the mixture with CCD at 25 °C for 45 min. SDS-PAGE analysis revealed that fusion protein was efficiently and selectively labeled with the fluorogenic probe (Figure 1c).

Finally, we investigated specific labeling of target proteins displayed on the surface of living cells. ^{E166N}TEM was fused to the N-terminus of epidermal growth factor receptor (EGFR), a membrane associated protein, and the construct was produced in HEK293T cells. After treatment with CCD (see Supporting Information), the cells were examined under a fluorescence microscope. Only cells producing the ^{E166N}TEM-EGFR fusion protein emitted cyan fluorescence as a consequence of specific labeling by the probe (Figure 2b–e).

In conclusion, we have developed a novel protein labeling system that combines a genetically modified β-lactamase with low molecular weight fluorogenic β-lactam probes. Through appropriate probe design, we succeeded in labeling proteins with a sensitive fluorophore in vitro and on living cells. In principle, this system does not require washing procedures to remove the unreacted probes after labeling. Furthermore, since the ^{E166N}TEM tag protein is absent in mammalian cells, it can be used for the specific labeling of proteins in higher eukaryotes. We anticipate that this labeling system will find wide application in the field of life science.

Acknowledgment. We thank Dr. Shahriar Mobashery at the University of Notre Dame for kindly providing TEM-1 plasmid. We also thank Dr. Robert E. Campbell at Alberta University, Dr. Gregor Zlokarnik at Vertex Pharmaceuticals, and Dr. Donald Hivert at ETH Zürich for helpful discussions. S.W. acknowledges a Global COE Fellowship of Osaka University. This work was supported in part by MEXT of Japan.

Supporting Information Available: Detailed experimental procedures and supplementary figures. This material is available free of charge via the Internet at http://pubs.acs.org.

References

(1) Chudakov, D. M.; Lukyanov, S.; Lukyanov, K. A. *Trends Biotechnol.* **2005**, *23*, 605–613.
(2) Griffin, B. A.; Adams, S. R.; Tsien, R. Y. *Science* **1998**, *281*, 269–272.
(3) Los, G. V.; et al. *ACS Chem. Biol.* **2008**, *3*, 373–382.
(4) Keppler, A.; Gendreizig, S.; Pick, H.; Vogel, H.; Johnsson, K. *Nat. Biotechnol.* **2003**, *21*, 86–89.
(5) Chen, I.; Howarth, M.; Lin, W.; Ting, A. Y. *Nat. Methods* **2005**, *2*, 99–104.
(6) Lin, C.-W.; Ting, A. Y. *J. Am. Chem. Soc.* **2006**, *128*, 4542–4543.
(7) Hauser, C. T.; Tsien, R. Y. *Proc. Natl. Acad. Sci. U.S.A.* **2007**, *104*, 3693–3697.
(8) Ojida, A.; Honda, K.; Shinmi, D.; Kiyonaka, S.; Mori, Y.; Hamachi, I. *J. Am. Chem. Soc.* **2006**, *128*, 10452–10459.
(9) Waley, S. G. *In the chemistry of β-lactams*; Page, M. I., Ed.; Chapman & Hall: London, 1992; p 198.
(10) (a) Moore, J. T.; Davis, S. T.; Dev, I. K. *Anal. Biochem.* **1997**, *247*, 203–209. (b) Zlokarnik, G.; Negulescu, P. A.; Knapp, T. E.; Mere, L.; Burres, N.; Feng, L.; Whitney, M.; Roemer, K.; Tsien, R. Y. *Science* **1998**, *279*, 84–88. (c) Gao, W.; Xing, B.; Tsien, R. Y.; Rao, J. *J. Am. Chem. Soc.* **2003**, *125*, 11146–11147. (d) Campbell, R. E. *Trends Biotechnol.* **2004**, *22*, 208–211. (e) Xing, B.; Khanamiryan, A.; Rao, J. *J. Am. Chem. Soc.* **2005**, *127*, 4158–4159.
(11) Sutcliffe, J. G. *Proc. Natl. Acad. Sci. U.S.A.* **1978**, *75*, 3737–3741.
(12) Matagne, A.; Lamotte-Blasseur, J.; Frére, J.-M. *Biochem. J.* **1998**, *330*, 581–598.
(13) Guillaume, G.; Vanhove, M.; Lamotte-Brasseur, J.; Ledent, P.; Jamin, M.; Joris, B.; Frére, J.-M. *J. Biol. Chem.* **1997**, *272*, 5438–5444.
(14) Adachi, H.; Ohta, T.; Matsuzawa, H. *J. Biol. Chem.* **1991**, *266*, 3186–3191.
(15) Vijayakumar, S.; Ravishanker, G.; Pratt, R. F.; Beveridge, D. L. *J. Am. Chem. Soc.* **1995**, *117*, 1722–1730.

JA8082285

DOI: 10.1002/anie.200806328

Molecular Imaging

Dual-Function Probe to Detect Protease Activity for Fluorescence Measurement and ^{19}F MRI**

*Shin Mizukami, Rika Takikawa, Fuminori Sugihara, Masahiro Shirakawa, and Kazuya Kikuchi**

Noninvasive molecular imaging techniques are important for understanding the actual mechanisms of biological systems. In biological sciences, especially those involving cellular systems, the most widely used imaging technique is fluorescence microscopy, because of its high sensitivity, high spatiotemporal resolution, and simple experimental procedure.[1] On the other hand, magnetic resonance imaging (MRI) is one of the most successful imaging techniques in the field of clinical diagnosis. As MRI can visualize deep regions of animal bodies,[2] application of MRI to in vivo imaging of biomolecules is attracting attention.[3] Several ^{1}H MRI probes have been developed to investigate pH values,[4] metal ions,[5] and enzyme activities.[6]

Recently, heteronuclear MRI has been attracting considerable attention as an alternative molecular imaging technique. One of the most promising nuclides for MRI is ^{19}F,[7] which has a high NMR sensitivity that is comparable to that of ^{1}H, and almost no intrinsic ^{19}F signals can be observed in living animals. ^{19}F MRI does not have the drawback of background signals from intrinsic biomolecules, which interfere with the probe signals. Very recently, we developed a novel design strategy for ^{19}F MRI probes that can detect protease activity.[8] We exploited the paramagnetic relaxation enhancement (PRE) effect to achieve off/on switching of the probe MRI signals (Scheme 1a). Using the ^{19}F MRI probe Gd-DOTA-DEVD-Tfb (Tfb = *para*-trifluoromethoxybenzyl) based on this mechanism, we were successful in detecting caspase-3 activity by ^{19}F MRI.

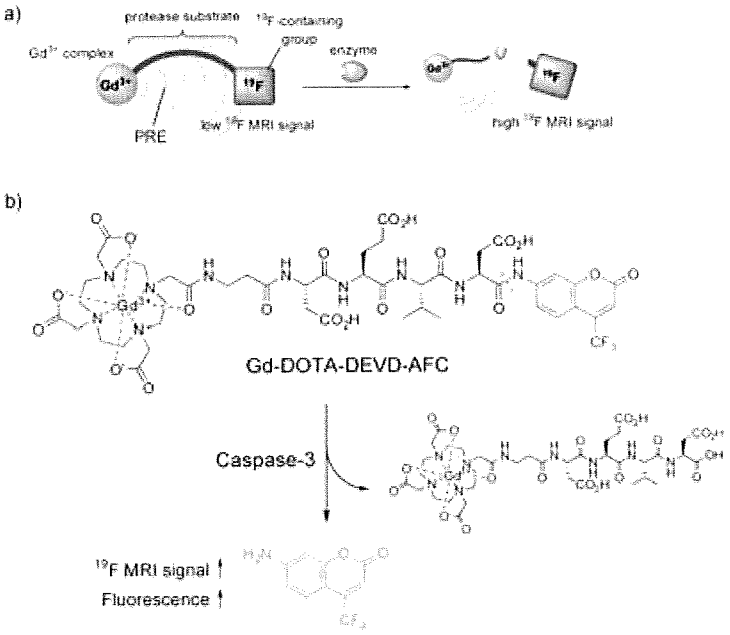

Scheme 1. a) Representation of ^{19}F MRI detection of protease activity. b) Chemical structure of Gd-DOTA-DEVD-AFC and its reaction scheme for detecting caspase-3 activity.

Although MRI can visualize deep regions of living bodies, its sensitivity is inferior to that of fluorescence measurement. The lower sensitivity requires longer accumulation time for imaging. If the probes are multifunctional, we can choose the appropriate imaging method in accordance with the experimental conditions. Higuchi et al. developed the dual-function probe (*E*,*E*)-1-fluoro-2,5-bis(3-hydroxycarbonyl-4-hydroxy)-styrylbenzene (FSB), which aggregates to amyloidβ (Aβ) plaques, for ^{19}F MRI and fluorescence measurements.[9] ^{19}F MRI signals localized on Aβ plaques were observed in living mice in vivo, and fluorescence signals in brain slices ex vivo.[9] As such complementary experiments have resulted in more reliable conclusions, development of multimodal imaging probes is very important.[10] Herein we report a dual-function probe to detect protease activity by fluorescence measurement and ^{19}F MRI that is based on the development of Gd-DOTA-DEVD-Tfb.[8]

We chose 7-amino-4-trifluoromethylcoumarin (AFC) as a reporter group that is active in both ^{19}F MRI and fluorescence measurement. AFC is strongly fluorescent in polar solvents,

[*] Dr. S. Mizukami, R. Takikawa, Prof. K. Kikuchi
Graduate School of Engineering
Osaka University, Osaka 565-0871 (Japan)
Fax: (+81) 6-6879-7924
E-mail: kkikuchi@mls.eng.osaka-u.ac.jp
Homepage: http://www-molpro.mls.eng.osaka-u.ac.jp/
F. Sugihara
International Graduate School of Arts and Sciences
Yokohama City University, Kanagawa 230-0045 (Japan)
Cellular & Molecular Biology Laboratory
RIKEN Advanced Science Institute
Saitama 351-0198 (Japan)
Prof. M. Shirakawa
Graduate School of Engineering
Kyoto University, Kyoto 615-8510 (Japan)
CREST, Science and Technology Corporation, Saitama 332-0012 (Japan)

[**] This work was supported in part by MEXT of Japan. MRI = magnetic resonance imaging.

Supporting information for this article is available on the WWW under http://dx.doi.org/10.1002/anie.200806328.

and the fluorescence properties of 7-aminocoumarin derivatives depend on the electron-donating ability of the 7-amino group.[11] Usually, the peptide modification on the 7-amino group induces a blue shift of the fluorescence spectrum with a decrease in fluorescence intensity. Thus, AFC has been utilized as the fluorophore for protease activity detection.[12] Furthermore, the ^{19}F NMR spectrum of AFC shows only a singlet peak without any coupling to intramolecular protons. AFC is thus appropriate for ^{19}F MRI.

We designed a bimodal probe Gd-DOTA-DEVD-AFC (Scheme 1), in which the probe consists of mainly three parts: Gd^{3+}-DOTA complex (DOTA = 1,4,7,10- tetraazacyclododecane-1,4,7,10-tetraacetate), caspase-3 substrate peptide (DEVD), and ^{19}F-containing fluorophore (AFC). When caspase-3 cleaves the C terminus of the DEVD sequence, AFC is produced. After the enzyme is cleaved, the ^{19}F MRI signal is increased in much the same manner as in Gd-DOTA-DEVD-Tfb (Scheme 1 a). Simultaneously, the fluorescence spectrum of AFC is increased. Thus, Gd-DOTA-DEVD-AFC is expected to work as a bimodal probe that detects caspase-3 activity.

The Gd-DOTA-DEVD-AFC probe was synthesized using Fmoc solid-phase chemistry, followed by complex formation with the Gd^{3+} ion (Scheme 2). The excitation peak of Gd-DOTA-DEVD-AFC is at 340 nm, and irradiation at 400 nm results in little fluorescence emission. The incubation of the probe with caspase-3 at 37 °C induced the excitation spectral shift toward longer wavelengths. Therefore, when the probe was excited at 400 nm, the emission at around 500 nm was substantially increased (Figure 1). From the fluorescence measurements, the kinetic parameters for hydrolysis of Gd-DOTA-DEVD-AFC by caspase-3 were measured. The V_{max}/K_m value of Gd-DOTA-DEVD-AFC is 7.61×10^{-3} s^{-1}. On the other hand, V_{max}/K_m of Ac-DEVD-AMC, the commercially available fluorescent substrate (AMC = 7-amino-4-methylcoumarin), is 9.91×10^{-4} s^{-1}. This result indicates that Gd-DOTA complex does not hinder the enzyme reaction at all. Thus, Gd-DOTA-DEVD-AFC can be used as a superior fluorogenic probe for detecting caspase-3 activity.

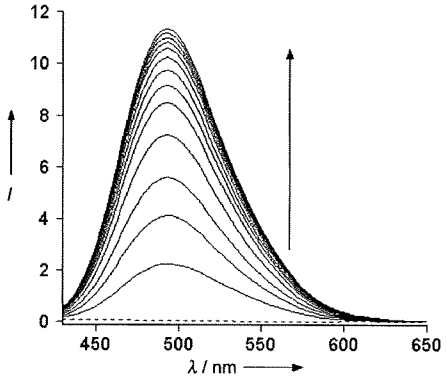

Figure 1. Time-dependent emission spectra of Gd-DOTA-DEVD-AFC (10 μM) with casapse-3 (0.84 mU) in the reaction buffer (pH 7.4) at 37 °C. The spectra were measured every 2 min after the addition of the enzyme. The dotted line indicates no caspase-3. The excitation wavelength: 400 nm. Reaction buffer: 4-(2-hydroxyethyl)-1-piperazineethanesulfonic acid (HEPES, pH 7.4, 50 mM) containing glycerol (10%), NaCl (100 mM), dithiothritol (DTT, 10 mM), ethylenediaminetetraacetic acid (EDTA, 1 mM), and 3-[(3-cholamidopropyl)dimethylammonio]-1-propanesulfonate (CHAPS, 0.1%).

We measured the ^{19}F NMR spectra of Gd-DOTA-DEVD-AFC and its metal-free analogue DOTA-DEVD-AFC. The NMR signal of Gd-DOTA-DEVD-AFC was broad and weak compared to that of the Gd^{3+}-free DOTA-DEVD-AFC (Supporting Information). This change in peak shape and intensity suggests that ^{19}F undergoes an intramolecular PRE effect from the Gd^{3+} ion. Longitudinal (T_1) and transverse (T_2) relaxation times of DOTA-DEVD-AFC (250 μM) were (0.479 ± 0.003) s and (0.152 ± 0.006) s, respectively (Table 1). In case of Gd-DOTA-DEVD-AFC, we could not estimate either T_1 or T_2, because these relaxation times were markedly shorter and the ^{19}F NMR signal intensity was low. From molecular modeling, the distance between the Gd^{3+} ion and the ^{19}F atom in the probe was estimated to be less than 25 Å. However, as the substrate peptide is flexible, the Gd^{3+} ion can be distributed in closer proximity to ^{19}F, such that the PRE effect works efficiently.

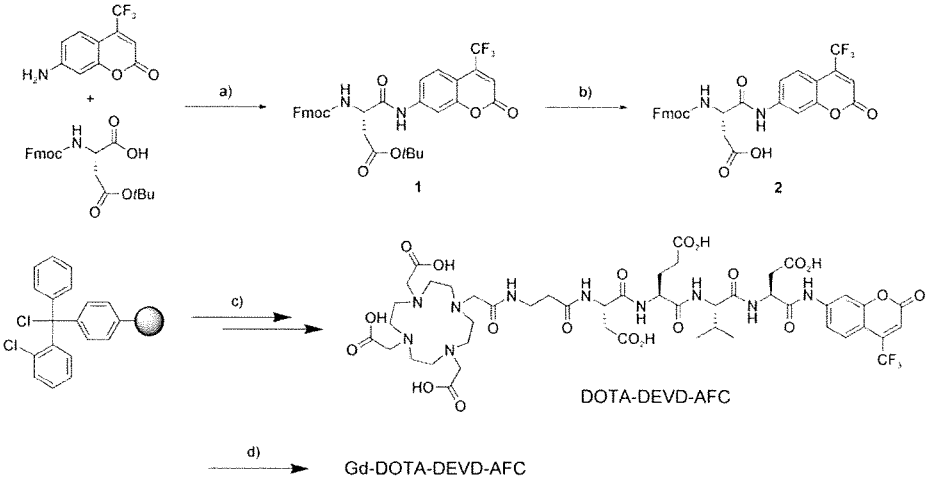

Scheme 2. Synthetic route to Gd-DOTA-DEVD-AFC. a) $POCl_3$, pyridine. b) trifluoroacetic acid. c) Fmoc peptide synthesis: **2**, Fmoc-Val-OH, Fmoc-Glu(O*t*Bu)-OH, Fmoc-Asp(O*t*Bu)-OH, Fmoc-β-Ala-OH, tris-*t*Bu-DOTA, deprotection. d) $GdCl_3 \cdot 6H_2O$, 100 mM HEPES buffer (pH 7.4). Fmoc = fluorenylmethyloxycarbonyl.

Next, we performed an enzyme assay using ^{19}F NMR spectroscopy. When Gd-DOTA-DEVD-AFC was treated with caspase-3 in the reaction buffer at 37 °C, a sharper and a more intense ^{19}F NMR signal was observed, with a slight downfield shift (Figure 2). T_1 and T_2 of the cleaved product (250 μM) were elongated to (0.38 ± 0.04) s and (0.097 ± 0.004) s, respectively (Table 1). This finding indicates that the intramolecular PRE effect from the Gd^{3+} ion to the ^{19}F atom was cancelled owing to the cleavage of the probe. After complete cleavage by

Table 1: Longitudinal and transverse relaxation times of synthesized probes.

	T_1 [s][a]	T_2 [s][a]
DOTA-DEVD-AFC	0.479(3)	0.152(6)
Gd-DOTA-DEVD-AFC	_[b]	_[b]
Gd-DOTA-DEVD-AFC + caspase-3	0.38(4)[c]	0.097(4)[c]

[a] Parenthesis denotes standard deviation ($n=3$). [b] The relaxation time was too short to be determined. [c] The relaxation times were measured after the enzyme (250 μM) reaction was complete.

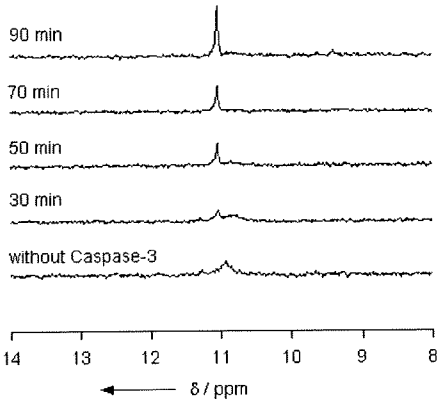

Figure 2. Time-dependent ^{19}F NMR spectra of Gd-DOTA-DEVD-AFC (250 μM) after addition of caspase-3 (1.25 mU) at 37 °C. Reaction buffer: As in Figure 1 plus D_2O (5%).

caspase-3 (confirmed by HPLC), the relaxation times T_1 and T_2 were lower than those observed for the metal-free ligand. These shorter relaxation times are most likely due to the intermolecular PRE of the cleaved Gd-DOTA (Supporting Information, Figure S4).

Finally, we attempted to visualize caspase-3 activity using a ^{19}F MRI phantom with Gd-DOTA-DEVD-AFC. Because of the extremely short relaxation time T_2, the ^{19}F MRI of Gd-DOTA-DEVD-AFC had no signals. When caspase-3 was added to the solution of Gd-DOTA-DEVD-AFC, augmentation of the ^{19}F MRI signal of the probe was observed (Figure 3).

In conclusion, we developed a novel dual-function probe, Gd-DOTA-DEVD-AFC, which detects caspase-3 activity by dual signal increase in fluorescence and in ^{19}F MRI. Because fluorescence measurement and MRI provide complementary information, such dual-mode probes should be quite useful for various biological experiments. Although several multimodal probes, such as fluorescence measurement and MRI, have been developed recently,[13] most probes are constructed by simple attachment of reporter moieties such as fluorescence dyes or MRI contrast agents. In contrast, multimodal probes accompanying plural signal enhancement have been scarcely reported. Such multimodal smart probes would be the next-generation probes in multimodal imaging for detecting enzyme activity.

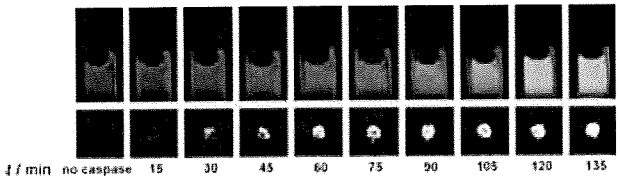

Figure 3. Time-dependent fluorescence images (top, λ_{ex}: 400 nm) and ^{19}F MR phantom images (bottom, diameter: approximately 2 mm) of Gd-DOTA-DEVD-AFC (10 μM for fluorescence measurement and 1 mM for ^{19}F MRI) with caspase-3 (60 nU for fluorescence measurement and 2 mU for ^{19}F MRI) at 37 °C. Reaction buffer: As in Figure 1. For ^{19}F MRI, [D_6]DMSO (20%) was introduced into the reaction buffer.

Received: December 26, 2008
Published online: April 7, 2009

Keywords: fluorescence · magnetic resonance imaging · molecular imaging · multimodal probe · proteases

[1] J. R. Lakovicz, *Principles of Fluorescence Spectroscopy*, 3rd ed., Springer Science & Business Media, New York, **2006**.
[2] a) A. Jasanoff, *Trends Neurosci.* **2005**, *28*, 120–126; b) D. E. Sosnovik, R. Weissleder, *Curr. Opin. Biotechnol.* **2007**, *18*, 4–10.
[3] R. Weissleder, M. J. Pittet, *Nature* **2008**, *452*, 580–589.
[4] a) S. Zhang, W. Kuangcong, A. D. Sherry, *Angew. Chem.* **1999**, *111*, 3382–3384; *Angew. Chem. Int. Ed.* **1999**, *38*, 3192–3194; b) S. Aime, A. Barge, D. D. Castelli, F. Fedeli, A. Mortillaro, F. U. Nielsen, E. Terreno, *Magn. Reson. Med.* **2002**, *47*, 639–648.
[5] a) W. Li, S. E. Fraser, T. J. Meade, *J. Am. Chem. Soc.* **1999**, *121*, 1413–1414; b) K. Hanaoka, K. Kikuchi, Y. Urano, M. Narazaki, T. Yokawa, S. Sakamoto, K. Yamaguchi, T. Nagano, *Chem. Biol.* **2002**, *9*, 1027–1032.
[6] a) A. Y. Louie, M. M. Hüber, E. T. Ahrens, U. Rothbächer, R. Moats, R. E. Jacobs, S. E. Fraser, T. J. Meade, *Nat. Biotechnol.* **2000**, *18*, 321–325; b) J. M. Perez, L. Josephson, T. O'Loughlin, D. Högemann, R. Weissleder, *Nat. Biotechnol.* **2002**, *20*, 816–820; c) B. Yoo, M. D. Pagel, *J. Am. Chem. Soc.* **2006**, *128*, 14032–14033; d) J. W. Chen, M. Q. Sans, A. Bogdanov, R. Weissleder, *Radiology* **2006**, *240*, 473–481.
[7] J. Yu, V. D. Kodibagkar, W. Cui, R. P. Mason, *Curr. Med. Chem.* **2005**, *12*, 819–848.
[8] S. Mizukami, R. Takikawa, F. Sugihara, Y. Hori, H. Tochio, M. Wälchli, M. Shirakawa, K. Kikuchi, *J. Am. Chem. Soc.* **2008**, *130*, 794–795.
[9] M. Higuchi, N. Iwata, Y. Matsuba, K. Sato, K. Sasamoto, T. C. Saido, *Nat. Neurosci.* **2005**, *8*, 527–533.
[10] a) E. A. Schellenberger, D. Sosnovik, R. Weissleder, L. Josephson, *Bioconjugate Chem.* **2004**, *15*, 1062–1067; b) Y. M. Huh, Y. W. Jun, H. T. Song, S. Kim, J. S. Choi, J. H. Lee, S. Yoon, K. S. Kim, J. S. Shin, J. S. Suh, J. Cheon, *J. Am. Chem. Soc.* **2005**, *127*, 12387–12391; c) P. Sharma, S. Brown, G. Walter, S. Santra, B. Moudgil, *Adv. Colloid Interface Sci.* **2006**, *123–126*, 471–485; d) J. H. Choi, F. T. Nguyen, P. W. Barone, D. A. Heller, A. E. Moll, D. Patel, S. A. Boppart, M. S. Strano, *Nano Lett.* **2007**, *7*, 861–867.
[11] C. E. Wheelock, *J. Am. Chem. Soc.* **1959**, *81*, 1348–1352.
[12] R. E. Smith, E. R. Bissel, A. R. Mitchell, K. W. Pearson, *Thromb. Res.* **1980**, *17*, 393–402.
[13] a) Y. M. Huh, Y. W. Jun, H. T. Song, S. Kim, J. S. Choi, J. H. Lee, S. Yoon, K. S. Kim, J. S. Shin, J. S. Suh, J. Cheon, *J. Am. Chem. Soc.* **2005**, *127*, 12387–12391; b) J. H. Lee, Y. W. Jun, S. I. Yeon, J. S. Shin, J. Cheon, *Angew. Chem.* **2006**, *118*, 8340–8342; *Angew. Chem. Int. Ed.* **2006**, *45*, 8160–8162; c) S. A. Corr, Y. P. Rakovich, Y. K. Gun'ko, *Nanoscale Res. Lett.* **2008**, *3*, 87–104; d) K. Tanaka, K. Inafuku, Y. Chujo, *Bioorg. Med. Chem.* **2008**, *16*, 10029–10033.

DOI: 10.1002/cbic.200900214

Development of Ratiometric Fluorescent Probes for Phosphatases by Using a pK_a Switching Mechanism

Shin Mizukami, Shuji Watanabe, and Kazuya Kikuchi*[a]

The use of fluorescent probes in fluorimetric assays is particularly useful in physiological studies because of their high sensitivity and noninvasiveness. For example, the widely used Ca^{2+} probe fura-2[1] and the subsequently developed fluorescent probes[2] have contributed significantly to the rapid progress of intracellular Ca^{2+} signaling studies. One of the outstanding characteristics of fura-2 is that it exhibits a shift in its excitation spectra in response to changes in Ca^{2+} concentration, which enables ratiometric fluorescence measurement at two wavelengths. Ratiometric measurement, in which the fluorescence intensity is monitored at two excitation or two emission wavelengths and the ratio of the two values is calculated, is more practical than normal fluorescence intensity measurement, because ratiometric measurement can exclude such variables as the influence of dye localization and fluctuation of excitation light intensity.[3]

For the rational design of ratiometric fluorescent probes, the resonance energy transfer (RET) mechanism is quite useful.[4] However, small-molecule RET probes generally require complicated synthesis, which involves conjugation of two different fluorescent dyes. Therefore, a new design principle for ratiometric probes is required. In this study, we developed a novel design strategy for ratiometric fluorescent probes. We applied this strategy in the development of fluorescent probes for detecting phosphatase activity.

Phosphatases catalyze the dephosphorylation of various types of biomolecules, including proteins, nucleic acids, and lipids, and play significant roles in the regulation of metabolic pathways in living organisms. Phosphatases are categorized into several groups, including alkaline phosphatases (ALP),[5] acid phosphatases (ACP),[6] serine/threonine phosphatases,[7] and tyrosine phosphatases (PTP)[8] to name a few. Thus far, several fluorescent probes have been developed for detecting phosphatase activity.[9–12] One prototype is 4-methylumbelliferyl phosphate (MUP),[9] which is hydrolyzed by several types of phosphatases, resulting in an increase in the fluorescence intensity. Other fluorescent phosphatase probes such as 3,6-fluorescein diphosphate (FDP)[10] and 6,8-difluoro-4-methylumbelliferyl phosphate (DiFMUP)[11] are also widely used. However, these probes do not have ratiometric fluorescence properties. Thus, the development of ratiometric fluorimetric probes that can detect phosphatase activities has been attempted by many research groups.

In addition to the aforementioned limitation, known phosphatase probes have another drawback: they have an aryl phosphate monoester moiety; phosphodiesterases convert them to the corresponding aryl alcohol, which fluoresce more strongly than the phosphate monoesters. Although they are considered structural analogues of phosphotyrosine and are used as fluorescent probes for detecting tyrosine phosphatase activity,[11,12] they are hydrolyzed by serine/threonine phosphatases[13] and ALP/ACP.[13,14] Usually, several types of phosphatase are activated in biological samples. When known phosphatase probes such as DiFMUP are used for the detection of phosphatase activity, the output fluorescence signal represents the sum of the activities of several phosphatases. Therefore, there is a requirement for more specific probes for individual phosphatases. For developing a specific probe for a phosphatase, the design of the enzyme-recognizing structure is important. The known probes always require an aryl phosphate monoester structure, and this structural requirement imposes severe limitations on probe design. Herein we report a novel design strategy for fluorescent probes that have an alkyl phosphate monoester structure. We investigated the specificity of the synthesized probes toward several phosphatases and discuss the correlation between their structure and the kinetic parameters in reaction with ACP.

In our design of new ratiometric probes, we initially focused on the fluorescence properties of coumarins. Coumarins containing an electron-donating substituent at the 6- or 7-position generally fluoresce in aqueous solution and have been extensively used for the fluorescence detection of various enzyme activities.[9,11,13,15] In particular, 7-hydroxycoumarins (umbelliferones) have been widely used because they have strong fluorescence intensities and they are easily synthesized. One of their distinctive characteristics is that their fluorescence properties are affected by solution pH;[16] excitation wavelength maxima (λ_{ex}) are approximately 330 and 370 nm in acidic and alkaline solution, respectively (Figure 1 A). This is because the protonation of the 7-hydroxy group affects fluorescence. By varying the pK_a value of the 7-hydroxy group through judicious substitution, the relative proportion of the phenol and phenolate forms in a neutral buffered solution can be systematically varied. Thus, if the pK_a value of the 7-hydroxy group can be controlled by an enzymatic reaction, the excitation spectrum of coumarin would change in response to the enzyme activity.

The conventional approach to vary the pK_a values of 7-hydroxycoumarins involves substitution of the hydrogen atom at the 6- or 8-position with a halogen atom such as fluorine or chlorine; this substitution decreases the pK_a value by an induc-

[a] Dr. S. Mizukami, S. Watanabe, Prof. K. Kikuchi
Division of Advanced Science and Biotechnology
Graduate School of Engineering, Osaka University
2-1 Yamadaoka, Suita, Osaka, 565-0871 (Japan)
Fax: (+81) 6-6879-7924
E-mail: kkikuchi@mls.eng.osaka-u.ac.jp

Supporting information for this article is available on the WWW under http://dx.doi.org/10.1002/cbic.200900214.

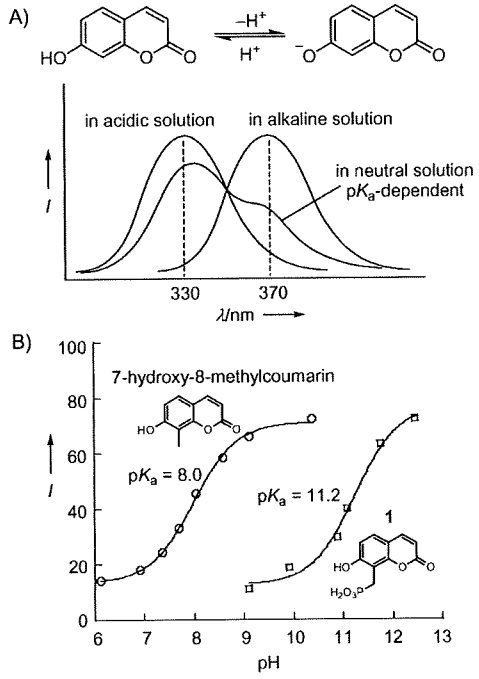

Figure 1. A) pH dependence of the excitation spectra of 7-hydroxycoumarin in aqueous solution (I = fluorescence intensity). B) Effect of a neighboring anionic group on the pK_a values of 7-hydroxycoumarins; fluorescence intensities were measured at λ_{ex} = 380 nm and λ_{em} = 470 nm (25 °C).

tive effect.[17] On the other hand, it has been reported that Calcein Blue (pK_a = 6.9[18]) and other 8-aminomethyl-substituted 7-hydroxycoumarins (pK_a = 6.6–6.7[19]) have lower pK_a values than 7-hydroxy-4-methylcoumarin (pK_a = 7.8[17]). In these cases, the positively charged ammonium groups probably interact with the 7-hydroxy group through hydrogen bonding or electrostatic interactions to enhance deprotonation. By extending this concept, we hypothesized that an anionic group at the 6- or 8-position might increase the pK_a value of the 7-hydroxy group in the opposite manner.

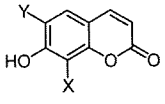

Compound	X	Y
1	$CH_2PO_3H_2$	H
2	$CH_2OPO_3H_2$	H
3a	$CH_2CH_2OPO_3H_2$	H
3b	CH_2CH_2OH	H
4a	H	$CH_2CH_2OPO_3H_2$
4b	H	CH_2CH_2OH
5a	$CH_2CH_2CH_2OPO_3H_2$	H
5b	$CH_2CH_2CH_2OH$	H

To confirm our hypothesis, we synthesized 7-hydroxy-8-phosphorylmethylcoumarin **1** (the synthesis is shown in Scheme S1 in the Supporting Information) and estimated the pK_a value from the fluorescence intensity at various pH values (Figure 1B). As expected, the pK_a value of **1** was considerably higher (pK_a = 11.2) than that of 7-hydroxy-8-methylcoumarin (pK_a = 8.0). This indicates a strong interaction between the anionic phosphate group and the 7-hydroxy group. We exploited this pK_a switch to develop a new type of fluorescent probe, as shown in Figure 2. Here, an anionic group is introduced in the coumarin scaffold at the 6- or 8-position through a tether to increase the pK_a value of the 7-hydroxy group.

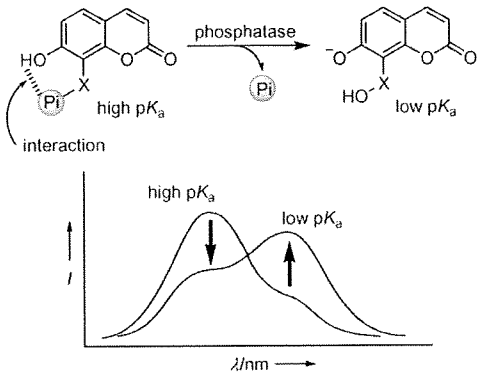

Figure 2. Change in the excitation spectrum of 7-hydroxycoumarin derivatives upon reaction with phosphatases (Pi: phosphate group, X: alkyl linker).

After enzymatic removal of this moiety, the pK_a value would decrease due to loss of the electrostatic interaction, resulting in a change in the excitation spectrum. We selected a phosphate group as the leaving anionic group. In this case, the probe can detect phosphatase activities.

We synthesized 7-hydroxy-8-phosphoryloxymethylcoumarin **2**. However, the compound was unstable and decomposed in aqueous solution. This is probably because the 7-hydroxy group accelerated the removal of the phosphate group to form quinone methide, as reported previously,[16] as phosphate is a good leaving group. We then synthesized **3a**, which has an 8-phosphoryloxyethyl group. We also synthesized **4a** and **5a** in order to examine the effect of the position of the anionic group and the alkyl chain length, respectively. Compounds **3b**–**5b**, lacking phosphate, were synthesized as control compounds. The synthetic routes are shown in Scheme S2 in the Supporting Information.

The pH dependence of the excitation spectrum of **3a** was measured (Figure 3A). Peaks were observed at 333 nm (pH 4.5) and 381 nm (pH 9.3). Between pH 6.5 and 9.3, the excitation spectrum has an isosbestic point at 350 nm; this indicates that only two species, the protonated and deprotonated forms of the 7-hydroxy group, are present in this pH range. The pK_a values of the 7-hydroxy groups of **3a** and **3b** were calculated to be 8.3 and 7.8, respectively, by curve fitting from plots of fluorescence intensity (λ_{ex} = 380 nm, λ_{em} = 470 nm) versus pH (Figure 3B). As we had hypothesized, **3a** showed a greater pK_a value than **3b**.

Compounds **4a** and **5a** showed similar pK_a values (8.1 and 8.2, respectively). The pK_a values of the corresponding dephosphorylated products **4b** and **5b** were 7.7 and 7.8, respectively. In each case, the pK_a value of the phosphate monoester is greater than that of the corresponding alcohol. On the basis of

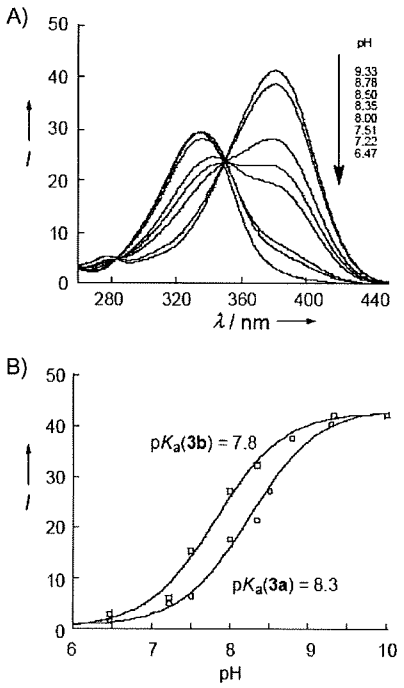

Figure 3. A) Change in the excitation spectrum of **3a** at various pH values (λ_{em} = 470 nm). B) Fluorescence intensities of **3a** (○) and **3b** (□) at various pH values (λ_{ex} = 380 nm, λ_{em} = 470 nm).

these results, it was expected that the excitation spectrum of **3a–5a** in neutral buffer solution would change after phosphatase-mediated dephosphorylation, as shown in Figure 2.

We examined the suitability of these compounds as fluorescence probes for phosphatases. When ACP was added to a 10 μM solution of **3a**, the excitation spectrum changed in the expected manner as a function of time. Compounds **4a** and **5a** showed similar spectral changes. For example, the excitation spectrum of **5a** shows a decrease at 330 nm and an increase at 380 nm (Figure 4), originating from the protonated and the deprotonated forms, respectively. The occurrence of the enzyme reaction was confirmed by HPLC (Figure S1, Supporting Information).

Next, we studied the reactivity of other phosphatases toward **3a**. As expected, **3a** was not dephosphorylated by PTPs (CD45 and PTP1B) or by serine/threonine phosphatases (PP1 and $PP2A_1$). On the other hand, ALP induced a partial change in the excitation spectrum of **3a**. However, the reaction rate decreased progressively as the reaction proceeded. This result suggests that the reaction product **3b** inhibits ALP activity. To confirm this putative product inhibition, we examined the effect of **3b** on the fluorescence intensity increase of a commercial fluorescent substrate, DiFMUP. The fluorescence intensity of DiFMUP increased significantly after the addition of ALP, whereas pre-incubation with **3b** inhibited this increase (Figure S2, Supporting Information). This supports the view that **3b** causes product inhibition. This inhibition was not observed with the other phosphatases we studied, so this may provide a clue to the development of selective ALP inhibitors. It is also noteworthy that some coumarin derivatives are protein kinase inhibitors.[17]

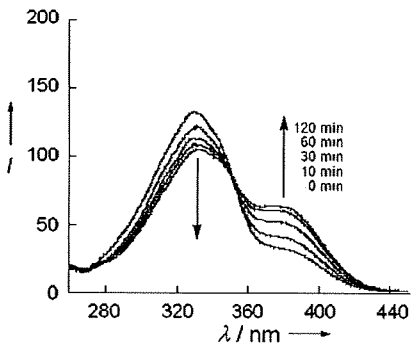

Figure 4. Excitation spectra of **5a** before and after the addition of ACP in 100 mM HEPES buffer solution (pH 7.4) (λ_{em} = 470 nm).

To examine the properties of the new fluorescent probes more quantitatively, we estimated the parameters K_M and V_{max} of ACP for **3a–5a** by fitting the plot of the initial velocity of the enzyme reaction versus substrate concentration with the Michaelis–Menten equation (Table 1). DiFMUP was used as the standard substrate under the same conditions. Among the three synthesized probes, **4a** and **5a** showed high V_{max}/K_M values, which were similar to that of DiFMUP, whereas **3a** was the worst substrate. The difference in the V_{max}/K_M values of **3a** and **4a** presumably reflects the difference in steric crowding around the phosphate group, because **3a** and **4a** are regioisomers; that is, **3a** is an 8-substituted coumarin and **4a** is a 6-substituted coumarin, and the 6-position of 7-hydroxycoumarin is less crowded than the 8-position. Compound **5a** had an additional methylene group in the linker, and it showed an approximate sixfold increase in the V_{max}/K_M value in comparison with **3a**. This finding indicates that further modification of the linker group might yield more selective and reactive fluorescent probes for ACP. Our design principle could also be used to develop specific probes not only for ACP but for other phosphatases as well.

Table 1. Kinetic parameters of **3a**, **4a**, and **5a** with acid phosphatase.[a]

Compound	K_M [μM]	$V_{max} \times 10^9$ [M min^{-1}]	V_{max}/K_M [min^{-1}]
3a	54 ± 18	4.7 ± 0.3	8.7×10^{-5}
4a	107 ± 27	53 ± 3	5.0×10^{-4}
5a	32 ± 12	17 ± 2	5.3×10^{-4}
DiFMUP	41 ± 19	31 ± 9	7.6×10^{-4}

[a] Kinetic data were measured at 30 °C in 100 mM HEPES buffer (pH 7.4) containing 1.0 mM DTT and 1.0 mM EDTA.

In conclusion, we have developed a novel design strategy using a pK_a switching mechanism for the design of ratiometric fluorescent probes to detect phosphatase activity. This design strategy is based on a pK_a shift of the 7-hydroxy group of 7-hydroxycoumarin derivatives induced by an adjacent anionic group, which is directly coupled to a change in the excitation spectrum. The synthesized probes are efficiently dephosphorylated by ACP, and changes in the excitation spectrum are ob-

